Research Paper

GEOSPHERE

GEOSPHERE, v. 21, no. 1

https://doi.org/10.1130/GES02778.1

10 figures; 1 table; 1 set of supplemental files

CORRESPONDENCE:
erin.e.donaghy@dartmouth.edu

CITATION: Donaghy, E.E., Eddy, M.P., Ridgeway, K.D., and Ickert, R.B., 2025, Sedimentary record of oceanic plateau accretion: Revisiting the Eocene to Miocene stratigraphy of the northern Olympic Peninsula, Washington (USA): Geosphere, v. 21, no. 1, p. 49–73, https://doi.org/10.1130/GES02778.1.

Science Editor: David E. Fastovsky
Associate Editor: Mark E. Holland

Received 25 March 2024
Revision received 30 August 2024
Accepted 31 October 2024

Published online 22 November 2024

Sedimentary record of oceanic plateau accretion: Revisiting the Eocene to Miocene stratigraphy of the northern Olympic Peninsula, Washington (USA)

Erin E. Donaghy, Michael P. Eddy, Kenneth D. Ridgway, and Ryan B. Ickert

Department of Earth, Atmospheric, and Planetary Sciences, Purdue University, West Lafayette, Indiana 47907, USA

ABSTRACT

Oceanic plateaus are common in modern oceanic basins and will ultimately collide with continental subduction zones. Despite the frequency of these events, complete sedimentary records of oceanic plateau collision and accretion have remained limited to only a few Cenozoic examples with excellent exposure and tectonic context. Our study focuses on building a stratigraphic record of plateau collision using the sedimentary strata deposited on the Siletzia oceanic plateau, which accreted to the Pacific Northwest at ca. 50 Ma. By combining previously published provenance and stratigraphic data with new lithofacies and geologic mapping, measured stratigraphic sections, conglomerate clast counts, and U-Pb zircon geochronology, we were able to divide the strata of the northern Olympic Peninsula in Washington, USA, into precollisional, syn-collisional, and postcollisional stages. Precollisional strata include early Eocene deep-marine hemipelagic to pelagic mudstones of the Aldwell Formation that were deposited directly on Siletzia basalts. These strata were deformed during collision and are separated from the overlying syn-collisional middle Eocene sandstone and conglomerate of the marine (?) Lyre Formation by an angular unconformity. Postcollisional strata were deposited by submarine fans and include interbedded sandstone and siltstone of the Hoko River and Makah formations. These units initially record the filling of isolated trench-slope basins by late Eocene time before eventual integration into an Oligocene regional forearc basin as the accreted Siletzia plateau began to subside. Our chronostratigraphy permits the correlation of basin strata across tectonic domains and provides more general insight into how forearc sedimentary systems evolve following the accretion of a young, buoyant oceanic plateau.

INTRODUCTION

Oceanic plateaus are large areas (>2 × 10^5 km^2) of overthickened (up to 38-km-thick) mafic crust that form in ocean basins and are frequently considered to be the magmatic manifestation of mantle plumes. These features are common in modern ocean basins with ages extending back to the Cretaceous (Kerr and Mahoney, 2007; Kerr, 2014). In addition, older accreted plateau fragments, now exposed on continental margins, demonstrate that they have been common for much of Earth's history and that accretion is an important process in the growth of continents (Kerr et al., 2003; Kerr, 2014; Kerr and Tarney, 2005; Taylor, 2006; Greene et al., 2010). The accreted plateaus also highlight that their ultimate fate is to collide with subduction zones as oceanic basins are consumed. These collisional events can lead to wholesale accretion of the oceanic plateau (e.g., Davy et al., 2008), accretion of the plateau's volcanic carapace (e.g., Mann and Taira, 2004), and the plateau's complete subduction (e.g., Liu et al., 2010), depending on its thickness and age, which are directly related to buoyancy and strength (Cloos, 1993; Mason et al., 2010; Vogt and Gerya, 2014; Tao et al., 2020; Liu et al., 2021).

Early Eocene collision of the Siletzia plateau with the North American Pacific Northwest led to its wholesale accretion (Wells et al., 2014; Anderson et al., 2024), which terminated a long-lived Cretaceous–Paleogene subduction zone and set the stage for the development of the modern Cascadia arc (Darin et al., 2022; Tepper and Clark, 2024). Available geochronology suggests that the plateau formed synchronously with its attempted subduction (Wells et al., 2014; Eddy et al., 2016, 2017), and it likely represents an endmember for plateau collisions in which the plateau is young, buoyant, and weak. Recent work in Washington, USA, has focused on the response of the upper plate to the accretion of the Siletzia plateau (Eddy et al., 2016, 2017; Wells et al., 2014; Miller et al., 2023), yet few studies have aspired to understand the sedimentary and tectonic response within the accreting plateau itself. On the Olympic Peninsula of western Washington, Cenozoic sedimentary and volcanic strata were deposited in a regional basin that directly overlies the basement basalts that comprise Siletzia and have long been known as the "peripheral rock sequence" (Fig. 1; Rau, 1964, 1966; Cady, 1975; Tabor and Cady, 1978a, 1978b; Snavely et al., 1986). Although these strata have been thoroughly studied, no previous research has integrated their depositional and structural history into the context of Siletzia's collision with the continental margin. The location of these strata on the Siletzia terrane makes it a prime candidate for gaining a better understanding of precollisional, syn-collisional, and postcollisional basin

Erin Donaghy https://orcid.org/0009-0005-9002-1036

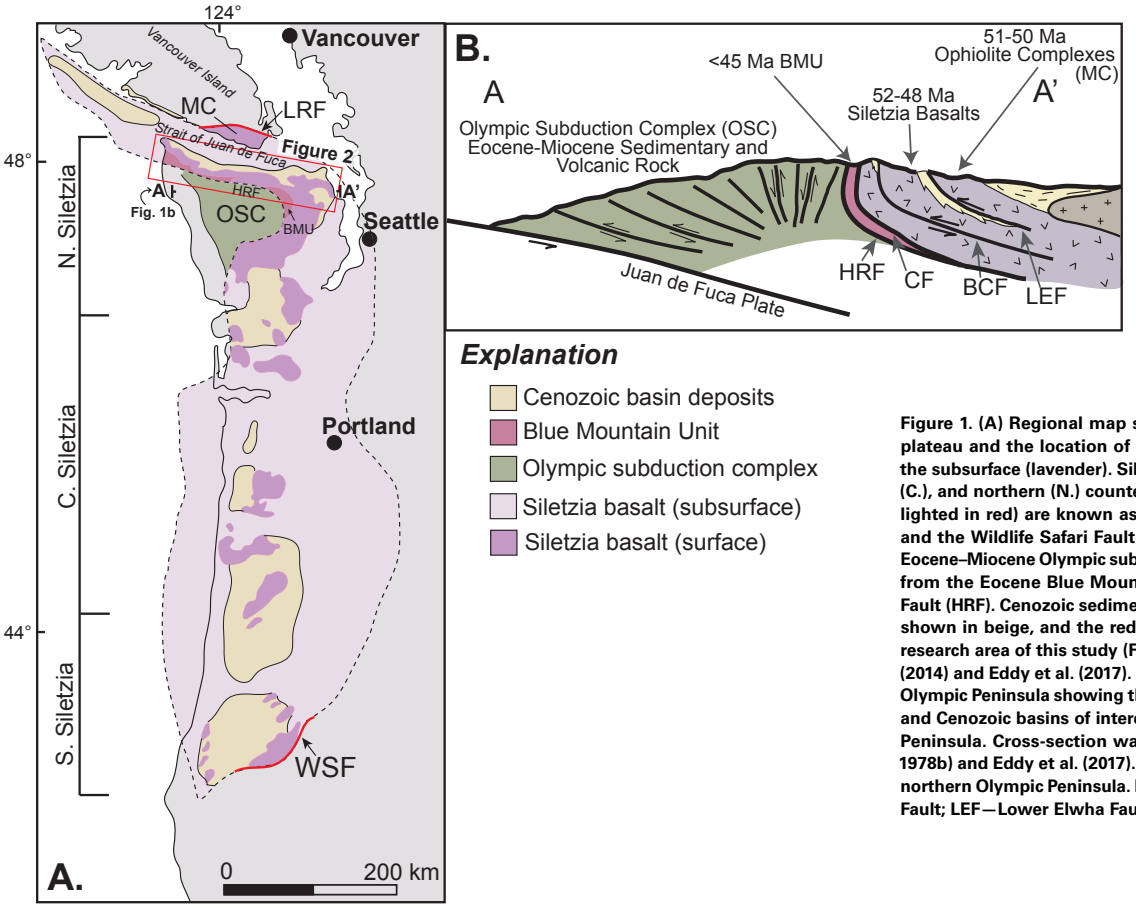

Figure 1. (A) Regional map showing the area of the Siletzia oceanic plateau and the location of its basalts at the surface (purple) and in the subsurface (lavender). Siletzia is divided into southern (S.), central (C.), and northern (N.) counterparts; the terrane boundary faults (highlighted in red) are known as the Leech River Fault (LRF) in the north and the Wildlife Safari Fault (WSF) in the south. Green indicates the Eocene–Miocene Olympic subduction complex (OSC), and it is separated from the Eocene Blue Mountain Unit (BMU) by the Hurricane Ridge Fault (HRF). Cenozoic sedimentary basins that sit on top of Siletzia are shown in beige, and the red box highlights the basin of interest and research area of this study (Fig. 2). Map was modified from Wells et al. (2014) and Eddy et al. (2017). (B) Present-day cross-section through the Olympic Peninsula showing the relationship of the OSC, Siletzia basalts, and Cenozoic basins of interest in this study on the northern Olympic Peninsula. Cross-section was modified from Tabor and Cady (1978a, 1978b) and Eddy et al. (2017). See Figure 2 for locations of faults on the northern Olympic Peninsula. BCF—Boundary Creek Fault; CF—Crescent Fault; LEF—Lower Elwha Fault; MC—Metchosin Complex.

evolution as the convergent margin transitioned from a long-lived Cretaceous–Paleogene subduction zone to the modern Cascadia arc. This record also provides a template for understanding the sedimentary response to the accretion of a young, buoyant, and weak oceanic plateau throughout the geologic record elsewhere in the world.

THE PERIPHERAL ROCK SEQUENCE ON THE NORTHERN OLYMPIC PENINSULA

Surface exposures of Siletzia in the Pacific Northwest are known as the Metchosin Complex on southern Vancouver Island, the Crescent Formation on the Olympic Peninsula, and the Siletz River Volcanic Formation in southern Washington and Oregon, USA (Fig. 1; Massey, 1986; Trehu et al., 1994; Wells et al., 2014; Phillips et al., 2017; Ciborowski et al., 2020). Geophysical evidence shows that Siletzia basalts reach up to 30 km thick in Oregon (Clowes et al., 1987; Trehu et al., 1994), are 18 km thick in Washington (Trehu et al., 1994), and thin to ~6 km along southern Vancouver Island (Hyndman et al., 1990). It is also geophysically continuous with a seismic anomaly under eastern Washington that is interpreted to represent subducted oceanic lithosphere (Gao et al., 2011; Schmandt and Humphreys, 2011). The terrane accreted during the early Eocene, and the suture between Siletzia and North America is exposed on Vancouver Island as the Leech River Fault zone and in Oregon as the Wildlife Safari Fault (Groome et al., 2003; Wells et al., 2000, 2014). Accretion was associated with the development of short-lived regional fold-and-thrust belts on Vancouver Island, Washington, and in Oregon (Tabor et al., 1984; Johnson, 1985; Wells

et al., 2014; Johnston and Acton, 2003; Eddy et al., 2016; Miller et al., 2016). This period of deformation is also recorded in nonmarine sedimentary basins exposed in central Washington. Basin strata record a reversal in paleoflow during the collision of Siletzia, followed by fold-and-thrust belt deformation and development of an unconformity (Eddy et al., 2016).

On the Olympic Peninsula in Washington, the Siletzia plateau is exposed as the Crescent Formation (Snavely et al., 1968; Duncan, 1982; Wells et al., 1984; Clark, 1989; Babcock et al., 1992). This formation was divided into lower and upper units of basalt on the basis of flow morphology (Tabor and Cady, 1978a, 1978b; Babcock et al., 1992, 1994), and was previously considered to represent a 16-km-thick section of stratigraphically continuous basalt (Trehu et al., 1994). The lowermost Crescent Formation was also interpreted to be interbedded with continentally derived turbidites in the Blue Mountain Unit (Brandon and Massey, 1985; Massey, 1986; Einarsen, 1987). These interpretations led many to consider the Crescent Formation as representative of a rift sequence rather than an accreted terrane. However, U-Pb detrital zircon geochronology has since shown that the Blue Mountain Unit is <45 Ma and younger than the overlying Crescent Formation (56–48 Ma), and that the two units must be structurally juxtaposed (Eddy et al., 2017). Given the possibility that the Crescent Formation is also structurally duplicated, we have abandoned its subdivision into lower and upper units and instead divide it based on flow morphology in Figure 2.

Overlying the Crescent basalts are Eocene–Miocene sedimentary strata known as the peripheral rock sequence (Tabor and Cady, 1978a, 1978b; Snavely et al., 1986; Garver and Brandon, 1994; Stewart and Brandon, 2004; Fig. 2). The northern peripheral rock sequence is exposed along the northern Olympic Peninsula and is distinct from the sedimentary strata that overlie Siletzia along the southern Olympic Peninsula (Snavely et al., 1980; Rau, 1964), where the Eocene is largely missing from the stratigraphic record (Tabor and Cady, 1978a, 1978b). The northern sequence has a more complete stratigraphic record that includes thick packages of early Eocene to Miocene sedimentary strata. Our study focuses on the stratigraphically lowest units in this sequence because they most likely record basin evolution before, during, and immediately after the accretion of Siletzia. These strata include, in ascending stratigraphic order, the Aldwell, Lyre, Hoko River, and Makah formations. Collectively, they are up to 6 km thick and record deposition in a variety of deep-marine depositional environments. They are overlain by the Oligocene–Miocene Pysht and Clallam formations, which were not the focus of this study and will not be discussed further.

The northern peripheral sequence rocks are exposed within several thrust sheets and associated folds along the northern Olympic Peninsula (Fig. 2). Existing depositional age constraints largely come from biostratigraphic data (Rau, 1964, 1966; Snavely et al., 1986), which permitted assignment of these formations to the Eocene and Oligocene, but does not provide sufficiently precise constraints to make detailed stratigraphic correlations across different structural domains. To improve our understanding of the depositional ages and timing of deformation recorded in these rocks, we supplemented existing lithologic and stratigraphic observations with our own mapping and geochronologic data to reconstruct the Eocene–Oligocene sedimentary, structural, and volcanic history of this region in the context of oceanic plateau accretion.

METHODS

Stratigraphic and Clast Compositional Data

We measured seven stratigraphic sections in the Sekiu River, Hoko River, Lower Elwha, and Dungeness areas and produced two new 1:18,000-scale lithofacies maps of the Lake Crescent and Dry Hills areas. Areas were targeted to constrain lateral and temporal variations in lithofacies of the Aldwell, Lyre, and Hoko River formations. These units are the lowermost part of the stratigraphic sequence and were targeted to constrain initial stages of basin development following oceanic plateau collision. Lithofacies were differentiated based on bed thickness, bed geometries, sedimentary structures, and composition. The resulting stratigraphic columns, facies descriptions, and lithofacies maps are presented in Tables SA1 and SA2 and Figures SA1–SA14 in the Supplemental Material.[1] Paleocurrent indicators in all units are rare to absent, but in general they suggest sediment derivation from the north, northwest, west, and northeast (Brown et al., 1956; Ansfield, 1972; Tabor and Cady, 1978a, 1978b; Snavely et al., 1980; DeChant, 1989; Shilhanek, 1992). Paleocurrents were not measured in this study either because they were absent or lacked significant numbers of high-confidence indicators.

In addition to the new stratigraphic data, we also supplemented previous petrographic descriptions of selected units with conglomerate clast compositional data. For each clast count, we randomly selected and identified clasts using an ~1 × 3 m grid surface within individual conglomerate beds. Some uncertainty exists regarding the identification of dark, fine-grained, pebble-sized clasts, and misidentification within this clast type could shift the compositional data by up to 10% among the igneous (e.g., basalt), metamorphic (e.g., argillite), and sedimentary (e.g., mudstone) fractions. However, this uncertainty does not affect the conclusions of this study. In addition to compositional data, we also measured the long axes of the ~10 largest clasts per conglomerate bed to determine the maximum particle size (Tables SB1–SB4, see footnote 1).

Coarse-grained sedimentary rocks are rare in most of the formations studied, and clast counts (N = number of clast count locations; n = number of individual clasts) are limited to the Aldwell (N = 2; n = 128), Lyre (N = 8; n = 924), and Hoko River (N = 1; n = 55) formations. The Lyre Formation received special emphasis since it is conglomeratic throughout the study area and

[1]Supplemental Material. Includes additional lithofacies characterization of the peripheral rock sequence (Tables SA1–SA2; Figs. SA1–SA14), conglomerate clast composition data (Tables SB1–SB4), geochemistry data (Table SC1), and geochronologic data (Tables SD1–SD3, SE1–SE10). Please visit https://doi.org/10.1130/GEOS.S.27616902 to view the supplemental material. Contact editing@geosociety.org with questions.

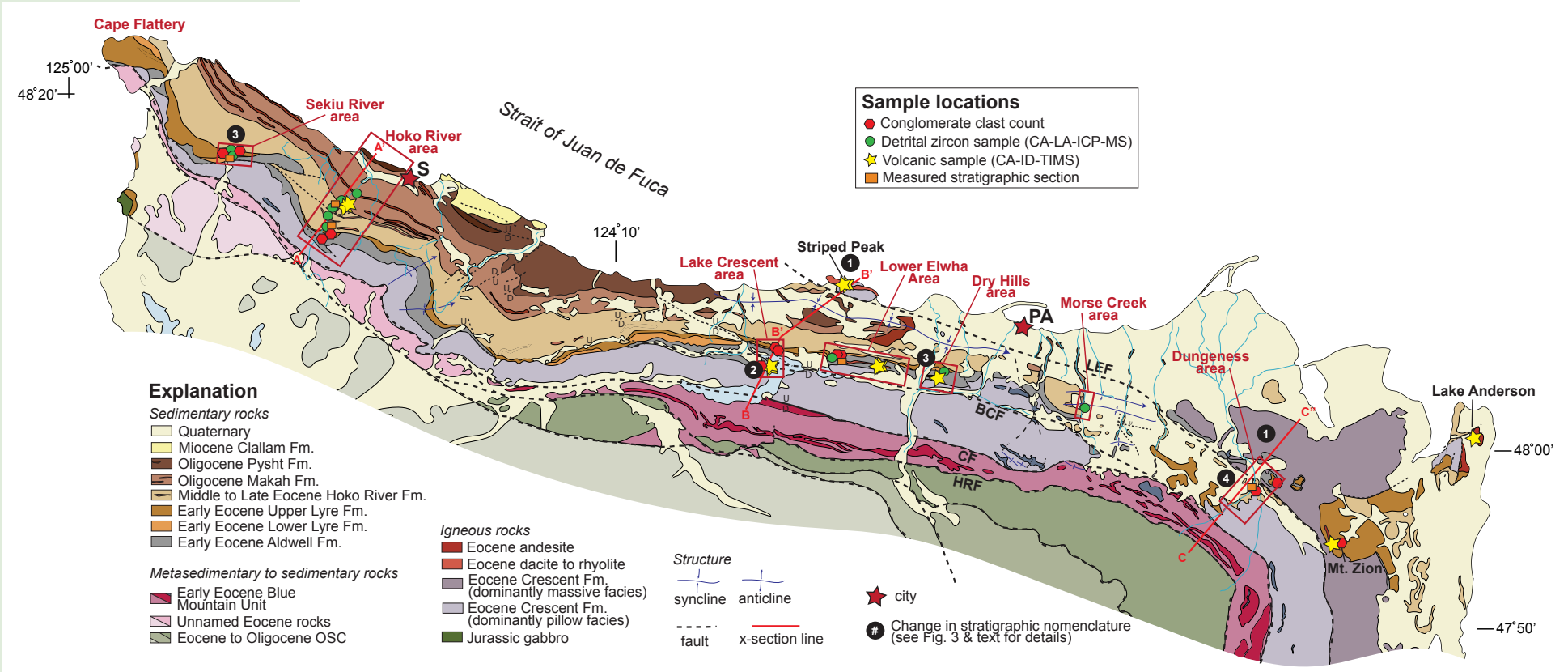

Figure 2. Regional geologic map of the northern Olympic Peninsula showing Eocene–Miocene sedimentary strata of the northern peripheral rock sequence. On average, these strata dip shallowly (5°–35°) to the north, except for where strata are exposed to adjacent folds and faults (Tabor and Cady, 1978a, 1978b; Snavely et al., 1986). Lowermost units (Aldwell and Lyre formations) especially show greater variability in structural orientation and dip of strata adjacent to regional faults (Supplemental Material, see text footnote 1). Research areas in this study are defined by the red boxes and sample type, and locations are shown. Cross-section lines are also defined by the labeled red lines in Figure 9. Black circled numbers represent areas of revised stratigraphic nomenclature based on new geochronologic data. Please see text and Figure 3 for more details. Map was modified from Tabor and Cady (1978a, 1978b). BCF—Boundary Creek Fault; CF—Crescent Fault; D—down; HRF—Hurricane Ridge Fault; LEF—Lower Elwha Fault; OSC—Olympic subduction complex; PA—Port Angeles; S—Sekiu; U—up. CA-LA-ICP-MS—chemical abrasion–laser ablation–inductively coupled plasma–mass spectrometry; CA-ID-TIMS— chemical abrasion–isotope dilution–thermal ionization mass spectrometry.

offered a chance to constrain lateral variations in provenance. For this reason, we conducted eight clast counts within the formation between the Sekiu River area and Mount Zion (Table SB2).

Geochronologic Data

We implemented two techniques of U-Pb zircon geochronology to better characterize depositional ages and sedimentary provenance: (1) chemical abrasion–isotope dilution–thermal ionization mass spectrometry (CA-ID-TIMS) of interbedded volcanic rocks, and (2) chemical abrasion–laser ablation–inductively coupled plasma–mass spectrometry (CA-LA-ICP-MS) of detrital zircons separated from sandstones. A total of 10 volcanic samples interbedded within the sedimentary peripheral rock sequence and two tuff samples from the underlying Crescent Formation were dated at Purdue University, West Lafayette, Indiana, USA (Fig. 3). Detailed methods for CA-ID-TIMS U-Pb zircon geochronology at Purdue University are presented in the Supplemental Material, and follow those outlined in Eddy et al. (2016) and Donaghy et al.

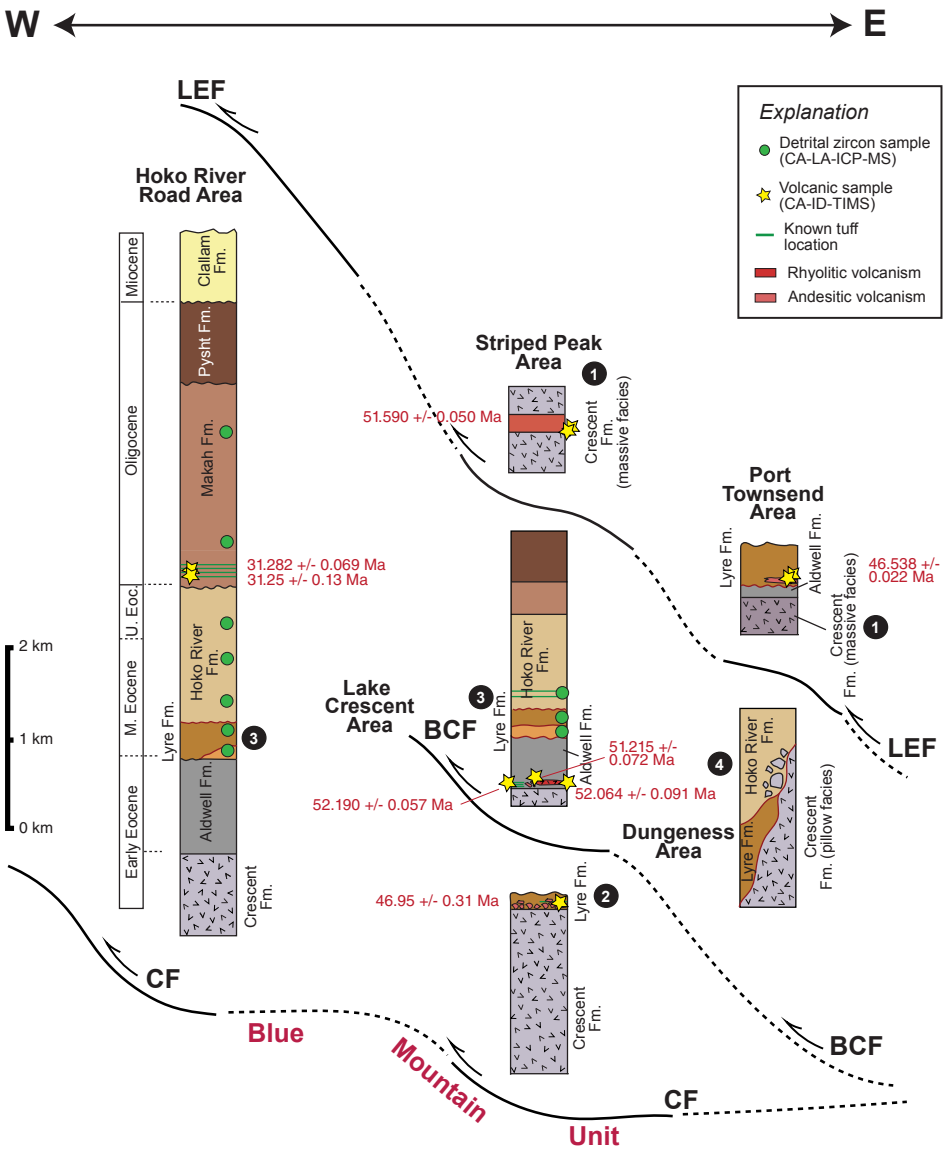

Figure 3. Generalized stratigraphic section of the Cenozoic peripheral rock sequence on the northern Olympic Peninsula. Port Townsend and Lake Crescent areas are split from age-equivalent strata on the northern Olympic Peninsula due to their locations in distinct fault blocks. Black circled numbers represent areas of revised stratigraphic nomenclature and new assignment of formations based on geochronologic data from this study. See text for details. BCF—Boundary Creek Fault; CF—Crescent Fault; LEF—Lower Elwha Fault; CA-LA-ICP-MS—chemical abrasion–laser ablation–inductively coupled plasma–mass spectrometry; CA-ID-TIMS—chemical abrasion–isotope dilution–thermal ionization mass spectrometry; U—upper; M—middle.

Revised Stratigraphy (this study)

1. Discontinue use of 'Lower' and 'Upper' subdivisions of the Crescent Fm.
2. Breccia of the Lyre Fm. mapped in the footwall of the BCF at Lake Crescent (previously mapped as Crescent/Aldwell Fm.)
3. Lower sandy mbr. of the Lyre Fm. mapped in the Dry Hills and along Sekiu River Rd. (previously mapped as Aldwell Fm.)
4. Lyre and Hoko River Fms. mapped in Dungeness Area (previously mapped as Blue Mountain Unit)

(2024). All isotopic data from these analyses and dates in this manuscript are reported with 2σ uncertainty (Tables SD1–SD3, see footnote 1).

The determination of eruption ages from CA-ID-TIMS U-Pb zircon data is challenging because increased precision has increasingly led to overdispersed $^{206}Pb/^{238}U$ dates in igneous samples. This overdispersion could arise through protracted pre-eruptive magma residence, the incorporation of xenocrysts during eruption, or underestimated laboratory uncertainties. Repeat measurements of a synthetic solution, ET100 (Condon et al., 2008), with a $^{206}Pb/^{238}U$ ratio equivalent to a zircon that is 100 Ma in age, give a weighted mean age of 100.130 ± 0.021 Ma (n = 10, mean square of weighted deviates [MSWD] = 2.7), which is similar to the values of this solution reported at other labs (Schoene et al., 2019; Schaltegger et al., 2021; Oliveira et al., 2023; Table SD3). To constrain eruption ages, we utilized the maximum likelihood age (MLA) model originally presented in Vermeesch (2021) as a method for identifying maximum depositional ages (MDAs). This approach assumes that the zircon data are drawn from a lognormal distribution that is truncated by a discrete age peak that corresponds to the eruption age. All interpretations of eruption ages from our CA-ID-TIMS U-Pb zircon data are reported in Table 1.

Detrital zircons were chemically abraded at Purdue University prior to LA-ICP-MS at the University of Arizona's LaserChron Center. The bulk chemical abrasion method is detailed in Donaghy et al. (2024; after Mattinson, 2005) and was implemented to selectively dissolve zones of Pb-loss that could skew zircon dates toward a younger apparent age (Nemchin and Cawood, 2005; Widmann et al., 2019; McKanna et al., 2023). All LA-ICP-MS U-Pb methods follow those reported in Pullen et al. (2018). Detrital zircons from the youngest peak age population were plucked from CA-LA-ICP-MS mounts for selected samples and dated by ID-TIMS to provide an MDA from parts of the stratigraphy without interbedded volcanic rocks (Table SD1). All geochronologic data determined using CA-LA-ICP-MS data is presented in Tables SE1–SE10 (see footnote 1).

DATA AND RESULTS

Our CA-ID-TIMS U-Pb zircon chronostratigraphy provides new, high-precision age control on strata of the peripheral rock sequence. As a result, we reconstructed detailed regional stratigraphic correlations between age-equivalent strata across numerous structural domains. This is essential for correlations across the northern Olympic Peninsula, where age-equivalent strata vary in lithology and are deformed by a series of major faults (Figs. 2 and 3). Our new chronostratigraphic framework in each thrust sheet allows better correlation of units across fault zones, providing a more detailed understanding of spatial and temporal changes in depositional environments as well as the timing and nature of different deformation events. Lithologic descriptions and CA-LA-ICP-MS U-Pb detrital zircon geochronology are reported below for each unit and interpreted in detail in the following discussion section.

Crescent Formation

We produced two CA-ID-TIMS U-Pb zircon eruption dates from tuffs interbedded within the Crescent Formation at Striped Peak, Washington, USA (Fig. 2). The Crescent Formation in this area is thrust over Eocene–Oligocene rocks of the peripheral rock sequence along the Lower Elwha Fault and consists of pillow basalt, hyaloclastite breccia, bioturbated basaltic sandstone, and

TABLE 1. RESULTS FROM U-Pb ZIRCON CA-ID-TIMS GEOCHRONOLOGY

Sample name	Formation	Location	Latitude (°N)	Longitude (°W)	Lithology	Th-corrected $^{206}Pb/^{238}U$ eruption date[a,c]	
OP20-ED-019A	Crescent Fm.	Striped Peak	48.1614	–123.6959	intermediate tuff; crystal-poor	51.590 ± 0.050 Ma (n = 7)	Eruption age
OP20-ED-019B	Crescent Fm.	Striped Peak	48.1614	–123.6959	intermediate tuff; crystal-rich	51.569 ± 0.073 Ma (n = 6)	Eruption age
OP20-ED-024	Aldwell Fm.	Dry Hills	48.0778	–123.5362	dacite	52.064 ± 0.091 Ma (n = 8)	Eruption age
092022ED06	Aldwell Fm.	Lake Crescent	48.0841	–123.7890	felsic tuff	52.190 ± 0.057 Ma (n = 7)	Eruption age
OP20-ED-052A	Aldwell Fm.	Eden Valley Road	48.0847	–123.6418	felsic volcanic (flow-banded)	51.215 ± 0.072 Ma (n = 5)	Eruption age
OP20-ED-052B	Aldwell Fm.	Eden Valley Road	48.0847	–123.6418	intermediate to felsic tuff	51.16 ± 0.12 Ma (n = 6)	Eruption age
OP20-ED-032	Lyre Fm.	Lake Anderson	48.0124	–122.7980	andesitic tuff/flow	46.559 ± 0.092 Ma (n = 8)	Eruption age
OP21-ED-141	Lyre Fm.	Mt. Zion	47.9266	–123.0150	andesite	46.584 ± 0.048 Ma (n = 8)	Eruption age
OP21-ED-143	Lyre Fm.	Mt. Zion	47.9266	–123.0150	andesite porphyry	46.538 ± 0.022 Ma (n = 5)	Eruption age
OP21-ED-028	Lyre Fm.	Lake Crescent	48.0827	–123.7893	intermediate to felsic tuff	46.95 ± 0.31 Ma (n = 8)	Eruption age
OP20-ED-015	Makah Fm.	Hoko River Road	48.2421	–124.3812	silicic tuff	31.25 ± 0.13 Ma (n = 6)	Eruption age
OP20-ED-014	Makah Fm.	Hoko River Road	48.2440	–124.3797	silicic tuff	31.282 ± 0.069 Ma (n = 7)	Eruption age
092222ED01A	Hoko River Fm.	Morse Creek	48.0414	–123.3496	volcaniclastic sandstone	43.96 ± 0.17 Ma (n = 4)[b]	MDA

Notes: CA-ID-TIMS—chemical abrasion–isotope dilution–thermal ionization mass spectrometry.
[a]Th correction was done using [Th/U] magma of 3.50.
[b]Maximum depositional age.
[c]Eruption date was calculated using methods outlined in Vermeesch (2021).

tuffaceous sedimentary strata (Fig. SA1). Both samples are from a sequence of 0.5–1-m-thick tuff beds and include a crystal-rich tuff (sample OP20-ED-019B) and a crystal-poor tuff (sample OP20-ED-019A). They yield U-Pb zircon eruption age estimates of 51.590 ± 0.050 Ma and 51.569 ± 0.073 Ma, respectively. Both ages are similar to a rhyolite dated ~50 km along strike to the east within massive basalt flows that are interpreted to have been erupted subaerially (Eddy et al., 2017). Given the same structural position of these rocks in the hanging wall of the Lower Elwha Fault and their contemporaneity (Fig. 2), the difference in depositional/eruptive environment may reflect lateral changes near the paleoshoreline. Alternatively, the massive flows that have been previously interpreted as subaerial could represent submarine sheet flows (Ballard et al., 1979), which can develop when the magmatic effusion rate is high, and magma viscosity is low (Gregg and Fink, 1995). Therefore, the differentiation of "Upper" and "Lower" Crescent Formation may be related more to variations in the depositional environment and/or proximity to the eruptive center rather than age, and we suggest dropping the terminology entirely (Fig. 3).

Precollisional Aldwell Formation

The Aldwell Formation is the lowermost unit in the peripheral rock sequence and consists primarily of massive mudstone. We measured stratigraphic sections and mapped lithofacies within the Aldwell Formation along the Sekiu River, Lake Crescent, Lower Elwha River Valley, and Dry Hills areas to characterize volcanic and sedimentary depositional environments (Figs. 2 and SA1–SA9). Overall, exposures of the Aldwell Formation are discontinuous, and the thickness varies along strike from up to 1 km thick to absent along the northern Olympic Peninsula (Fig. 2; Tabor and Cady, 1978a, 1978b; Marcott, 1984). Our new geologic mapping indicates that the contact with the underlying Crescent basalts is also variable along strike. Near the Hoko River on the northwestern Olympic Peninsula (Fig. 2), we mapped sheared mudstones of the Aldwell Formation in a brecciated zone with Crescent Formation basalt in the core of an anticline (Fig. 4A), which is consistent with previous mapping of a fault contact (Tabor and Cady, 1978a, 1978b; Snavely, 1987; Schasse, 2003). The contact has also been mapped as both unconformable (Brown et al., 1956; Snavely, 1987; Garver and Brandon, 1994) to conformable and interfingering with the underlying Crescent basalts (Brown and Gower, 1960; Tabor and Cady, 1978a, 1978b) at locations east of the Hoko River area. At Lake Crescent, we also observe the lowermost Aldwell Formation conformably overlying massive to pillow basalts of the Crescent Formation (Fig. SA5). Due to the poor exposure of this unit, the contact was not observed elsewhere.

The lowermost Aldwell Formation is characterized by a monolithic cobble–boulder basalt conglomerate that is no more than a few tens of meters thick (Brown and Gower, 1960; Snavely, 1987). Two conglomerate clast counts within this unit at Lake Crescent (n = 72 total clasts) and along the Hoko River (n = 56) are characterized by >95% basalt clasts (Table SB1). The Lower Aldwell Formation is also mapped with interbedded pods of felsic lava, basalt and tuff breccia, and water-lain lapilli tuff between the Lower Elwha and Lake Crescent areas on the central part of the northern Olympic Peninsula (Fig. 2; Brown and Gower, 1960; Schasse, 2003; and Tabor and Cady, 1978a, 1978b). We dated one of these felsic bodies in the Dry Hills (Fig. 2), and it yielded an eruption age of 52.064 ± 0.091 Ma (sample OP20-ED-024; Table 1). Whole-rock geochemistry of this sample indicates that it is dacitic in composition (Table SC1, see footnote 1). West of this location along strike with the dacite, a volcanic breccia with felsic to intermediate clasts is mapped within the Lower Elwha River area (Fig. 2). Two clasts dated from the breccia at this location yielded eruption ages of 51.215 ± 0.072 Ma (sample OP21-ED-052A) and 51.16 ± 0.12 Ma (sample OP21-ED-052B). Farther to the west, along Lake Crescent, a series of white-weathering tuffs are exposed in a sequence of rhythmically interbedded siltstone and fine-grained sandstone (Fig. SA11). One of the tuff beds yielded an age of 52.190 ± 0.057 Ma (sample 092022ED06), which matches the age of the interbedded dacite to the east.

Despite coarser deposits of the Lower Aldwell Formation, the majority (>90%) of the Formation is characterized by massive sections of thinly bedded, dark gray siltstone to claystone with thin interbeds of very fine-grained sandstone (Figs. 5A and 5B). Sedimentary structures are rare in the Aldwell Formation, although evidence of soft sediment deformation and concretions is frequent throughout the unit (Tabor and Cady, 1978a, 1978b; Snavely, 1983; Marcott, 1984). Laminated siltstone and claystone sequences are often tens of meters thick and appear as laterally continuous with sharp, planar bedding contacts (Figs. SA6 and SA9, see footnote 1). Lithic arenites to graywackes are generally 2–5 cm thick and contain abundant basaltic and sedimentary lithic fragments (Marcott, 1984). Based on sandstone composition, the Aldwell Formation can be split into two distinct facies: eastern sandstones enriched in basalt detritus, and western sandstones enriched in chert and argillite detritus (Marcott, 1984). However, based on new geochronologic data, we have assigned some of these western sandstones to the overlying Lyre Formation, as discussed in the next section.

Syn-Collisional to Postcollisional Lyre Formation

The Lyre Formation is up to 800 m thick, and its lenticular map pattern is unique compared to the distribution of other units across the northern Olympic Peninsula. We measured stratigraphic sections and completed lithofacies mapping of the Lyre Formation along the Sekiu River, Lake Crescent, Lower Elwha River Valley, and Dry Hills areas (Fig. 2; Figs. SA2 and SA4–SA6). The Lyre Formation is subdivided into a lower sandy member and an upper conglomeratic member (Brown et al., 1956; Tabor and Cady, 1978a, 1978b), and the thickness of both of these units is variable along strike on the northern Olympic Peninsula. Contact relationships between the members of the Lyre Formation and with the underlying Aldwell and Crescent formations are difficult to discern due to poor and limited exposure along rivers and roadcuts. North of Lake Crescent, we mapped an angular unconformity separating sandy

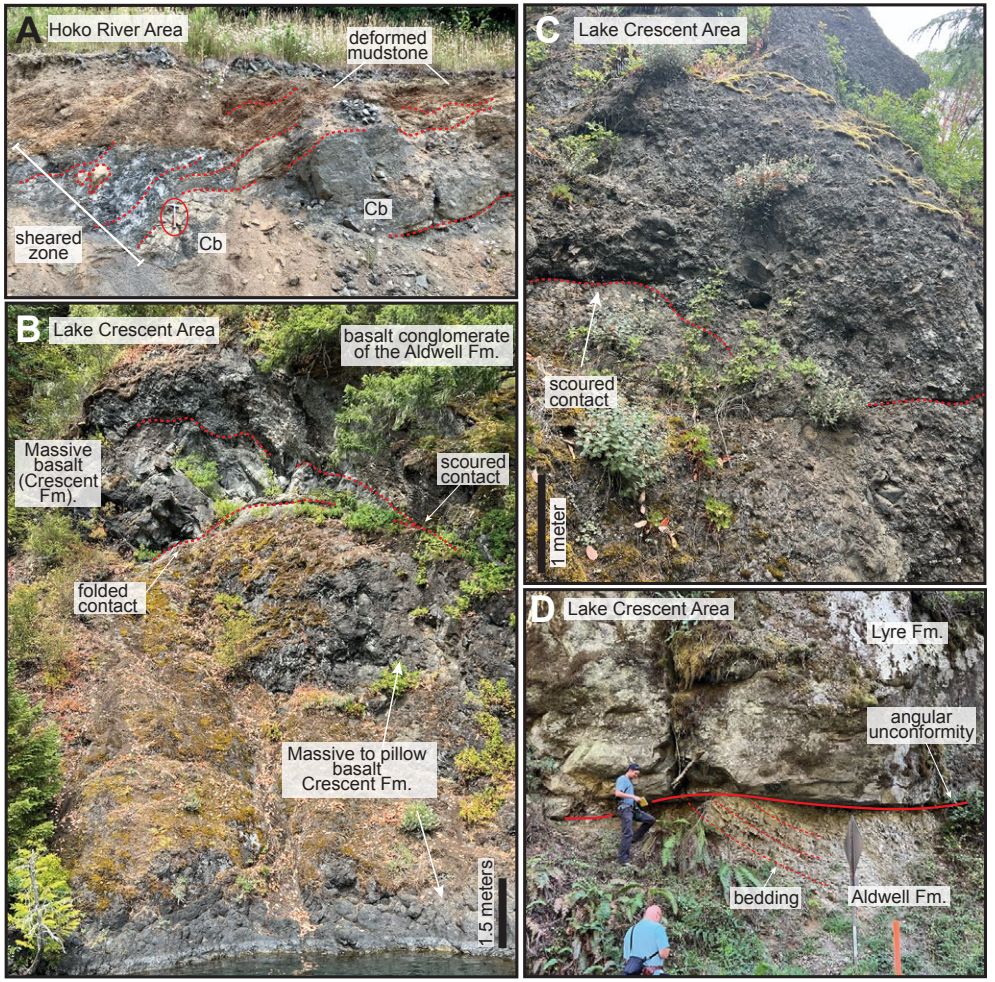

Figure 4. Photographs showing key contact relationships between the Crescent, Aldwell, and Lyre formations. (A) Sheared mudstone of the Aldwell Formation in fault contact with underlying Crescent Formation basalt (Cb) in the Hoko River area. Red dashed lines highlight sheared bedding contacts and basalt clasts (circled) that are suspended in the sheared mudstone matrix. Rock hammer is circled for scale. (B) Monolithic basalt conglomerate of the Aldwell Formation overlying massive to pillowed basalts of the Crescent Formation at Lake Crescent. Red dashed lines highlight contacts between units. (C) Massive monolithic basalt conglomerate of the Lower Aldwell Formation at Lake Crescent. Red dashed line highlights scoured contact between conglomerate beds. (D) Angular unconformity (solid red line) separating underlying folded mudstone of the Aldwell Formation from overlying sandy conglomerate of the Lower Lyre Formation north of Lake Crescent.

conglomerate and gravelly sandstone of the Lower Lyre Formation from underlying massive siltstone of the Aldwell Formation (Fig. 4D). A 20–30-cm-thick red weathering, clay-rich horizon is exposed along the surface of the unconformity and could represent a paleosol, although additional work is needed on this surface. This differs from previous mapping that suggests the Lyre Formation conformably overlies and interfingers the Aldwell Formation on the western Olympic Peninsula (Weaver, 1937; Brown et al., 1956). However, the stratigraphic intervals that comprise the Lyre Formation, especially the lower sandy member, have been redefined numerous times such that contact relationships with the Aldwell Formation remain uncertain (Brown et al., 1956). In contrast, previous researchers noted that conglomerate of the Upper Lyre Formation unconformably overlies strata of the Aldwell and Crescent formations where the lower sandy member is not present, which suggests an interval of erosion between members of the Lyre Formation (McWilliams, 1970).

The lower sandy member of the Lyre Formation is characterized by fine- to coarse-grained flaggy to massive sandstone interbedded with thinly laminated siltstone and sandy–gravel conglomerates (Figs. SA4 and SA6). Although sedimentary structures are rare, graded bedding and ripple cross-stratification are occasionally observed, and bed geometries appear to be planar and laterally continuous at the scale of the exposure (Fig. 5D; Brown et al., 1956). To help

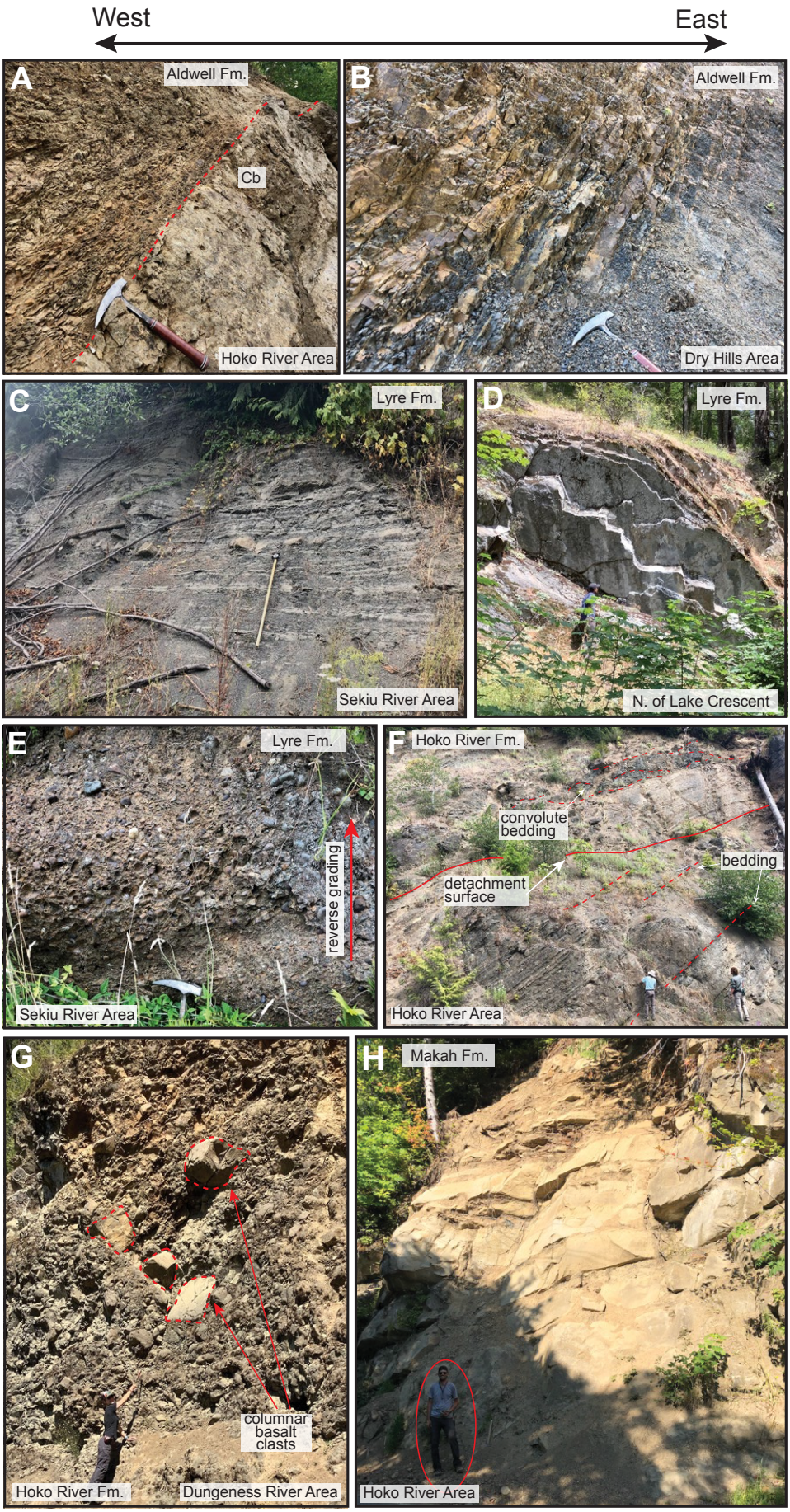

Figure 5. Photographs highlight key lithofacies of the northern peripheral rock sequence. (A) Fractured mudstone overlying Crescent Formation basalt (Cb) in the Hoko River area. (B) Thinly laminated mudstone of the Aldwell Formation in the Dry Hills area. (C) Interbedded sandstone and siltstone of the lower sandy member of the Lyre Formation exposed in the Sekiu River area. (D) Massive sandstone of the lower sandy member of the Lyre Formation exposed between Lake Crescent and the Dry Hills areas. (E) Massive cobble–boulder conglomerate of the upper conglomeratic member of the Lyre Formation exposed in the Sekiu River area. See hammer head for scale. (F) Thinly bedded siltstone and sandstone of the Hoko River Formation. Bedding (red dashed lines) in the lower part of the photograph trends into a well-defined detachment surface associated with postdepositional slumping of sediment. Convolute bedding is highlighted in the upper part of the photograph. People in lower right of photo are shown for scale. (G) Massive boulder conglomerate of the Lower Hoko River Formation along the Dungeness River. Note large clasts of columnar basalt. Person in lower left of photo is shown for scale. (H) Massive 1–1.5-m-thick feldspathic sandstone of the Makah Formation in the Hoko River area. Person in lower left of photo is circled for scale.

differentiate the Lower Lyre Formation from siltstones of the underlying Aldwell Formation, sandstone samples were collected for CA-LA-ICP-MS detrital zircon geochronology in the Sekiu River, Lower Elwha River, and Dry Hill areas (Fig. 2). In the Lower Elwha River area, the sandstone sample was collected from a well-known exposure of Lower Lyre Formation sandstones, rather than sampling locations with debated stratigraphic affiliation (Aldwell versus Lyre formations) in the Dry Hills (Polenz et al., 2004; Tabor and Cady, 1978a, 1978b) and Sekiu River areas (Brown et al., 1956; Shilhanek, 1992). Detrital zircon age spectra from the sandy member in the Lower Elwha River area (sample OP20-ED-028) look identical to samples collected in the nearby Dry Hills (sample OP20-ED-022) and along the Sekiu River (sample OP21-ED-015) to the west (Fig. 6A). Samples have five broadly defined peak age populations that are, in decreasing order of abundance, between 155 Ma and 160 Ma, 100 Ma and 130 Ma, 80 Ma and 100 Ma, 60 Ma and 75 Ma, and 180 Ma and 225 Ma. We note that the <100 Ma age populations are absent in the westernmost exposure of the lower sandy member (Fig. 6A). Based on the lithologic and geochronologic similarities of these strata, we modified previous mapping by Tabor and Cady (1978a, 1978b) to reflect the presence of the lower sandy member of the Lyre Formation at these locations (Sites 1 and 3 in Figs. 2 and 3).

The upper conglomeratic member of the Lyre Formation is characterized by matrix- to clast-supported pebble–cobble conglomerates (Fig. 5E; Fig. SA2). From east to west, there is a coarsening trend where pebble conglomerates grade to poorly sorted cobble–boulder conglomerates. At the northwesternmost point of the northern Olympic Peninsula, the Lyre Formation is mapped as the Cape Flattery breccia (Ansfield, 1972; Tabor and Cady, 1978a, 1978b; Snavely et al., 1986). The Cape Flattery breccia was not examined in this study, but is generally characterized by poorly sorted, massive boulder–cobble breccia to matrix-supported conglomerate that is interbedded with minor massive sandstone and siltstone (Snavely, 1983; Snavely et al., 1986; Shilhanek, 1992). A sandstone sample from the upper conglomeratic member of the Lyre Formation along the Sekiu River (n = 294; sample 092222ED04) yields broadly similar peak age populations compared to the underlying lower sandy member, but has a more significant ca. 50–56 Ma peak age population (Fig. 6A). Overall, all detrital zircon samples from the Lyre Formation had low-zircon yields, with only 200–300 zircon per 1–2 kg of sample processed.

Conglomerate clast counts were conducted along strike (Fig. 7) on the northern Olympic Peninsula to document how provenance changed spatially in the basin. Conglomerates in the western area along the Sekiu and Hoko rivers are dominated by igneous (40%–50% of total clasts) and metamorphic (20%–40%) clast types (Fig. 7). Metamorphic clast lithologies are mostly argillite and green metavolcanic rocks, whereas igneous clast types are characterized by gabbro, basalt, and dacite porphyry. Sedimentary clast compositions make up between 15% and 22% of total conglomerate clasts and are dominantly lithic-rich sandstones, siltstones, and chert. In the eastern Lyre Formation, conglomerates near Lake Crescent and the Elwha River Valley consist of primarily sedimentary (40%–55% of total clasts) and metamorphic (12%–30%) clast types. Sedimentary clasts are primarily reworked sandstone and chert, whereas metamorphic clasts are dominantly argillite, phyllite, and schist. In the hanging wall of the Lower Elwha Fault at Mount Zion and along the Dungeness River (Fig. 2), conglomerate clast compositions have similar proportions of sedimentary, igneous, and metamorphic rock types. However, in contrast to conglomerate clast compositions in the footwall of the Lower Elwha Fault, igneous types have a higher proportion of felsic to intermediate compositions (Fig. 7). Overall, there is an increase in the proportion of chert clasts in conglomerate to the east and an increase in metavolcanics and porphyritic dacite to the west. Sedimentary rocks make up a large percentage of conglomerate clast compositions at all locations, although they increase moderately from west (~20%–30% of all clasts) to east (~50% of all clasts). Igneous rocks (diorite, basalt, and gabbro) tend to make up equal proportions of conglomerate clast compositions at all locations (Fig. 7).

Of particular importance due to its location at the contact with the underlying Crescent Formation, a boulder breccia with clasts primarily comprising tuff is exposed along the western shore of Lake Crescent (Fig. 2). This volcanic breccia has previously been mapped as part of the Aldwell Formation (Brown and Gower, 1960) and Crescent Formation (Tabor and Cady, 1978a, 1978b), with its stratigraphic position remaining largely uncertain. Unlike the clast-supported monolithic basalt conglomerate of the lowermost Aldwell Formation, textures and fabric within this breccia indicate soft-sediment deformation and deposition by slumping and sliding (Fig. SA10). On average, angular clasts are >1.5–2 m in length and supported in a sheared mudstone matrix that folds around isolated clasts. A tuff clast interbedded in this breccia was sampled and dated using CA-ID-TIMS and yielded an age of 46.95 Ma ± 0.31 Ma (sample OP21-ED-028), which indicates that it is substantially younger than both the underlying Crescent and Aldwell formations (Fig. 3). Therefore, we remapped this tuffaceous breccia as part of the Lyre Formation based on our new age control (Site 2 in Figs. 2 and 3). Sandwiched between the tuff breccia and a chaotic assembly of massive basalt and matrix-supported boulder conglomerate is an isolated, 4–6-m-thick, coherent block of thinly bedded siltstone and mudstone (Fig. SA10). This block of coherent stratigraphy is identical to lithofacies of the Aldwell Formation and possibly represents an olistostromal block. Structural measurements and fault mapping along this transect indicate that these units are adjacent to a zone of complex faulting and folding that involves the underlying Aldwell and Crescent formations (Fig. SA5). Breccia beds mapped within this fault zone are characterized by angular pebble- to cobble-sized clasts in a white powdery matrix that resembles fault gouge and are mapped next to well-exposed fault planes. These faults have an average strike of 090–100 and dip ~45°–66° to the south toward a major north-dipping thrust that separates lowermost Aldwell Formation from the Lyre Formation breccia.

In the hanging wall of the Lower Elwha Fault, Lyre conglomerate of the upper member is interbedded with andesite and andesitic porphyry flows (Fig. 2). An andesitic tuff collected near Lake Anderson yielded a CA-ID-TIMS eruption age of 46.559 ± 0.092 Ma (sample OP20-ED-032) and is interbedded with gravelly sandstone and matrix-supported pebble conglomerate of the Lyre Formation (Table 1). Two volcanic samples were collected at Mount Zion

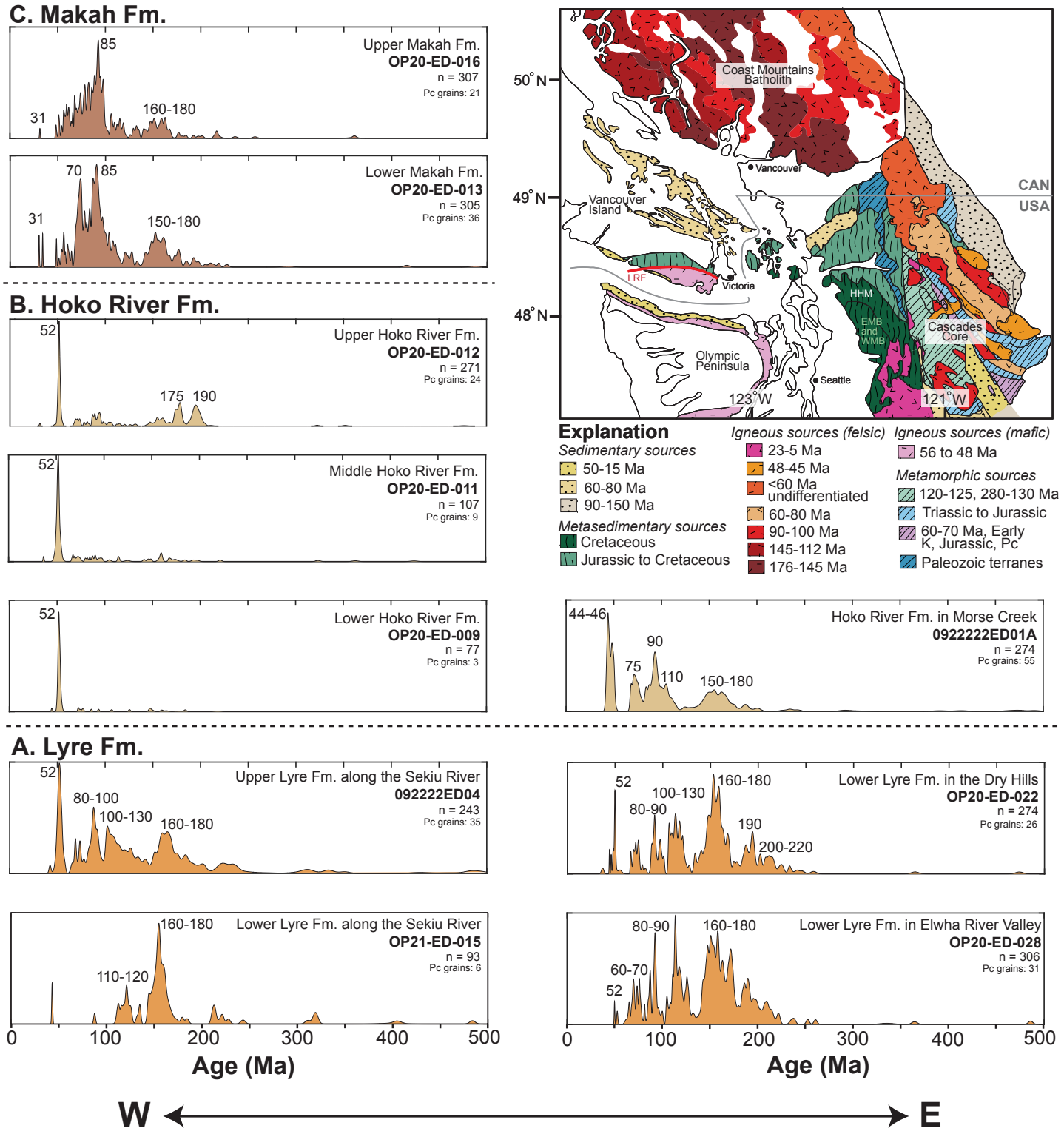

Figure 6. Probability density plots show the distribution of U-Pb age determinations for detrital zircon grains from (A) the Lyre Formation, (B) the Hoko River Formation, and (C) the Makah Formation. The map shows potential source terranes for detrital zircon grains. Map patterns and colors refer to specific age ranges and lithologies. EMB—Eastern Mélange Belt; HHM—Helena-Haystack Mélange; LRF—Leech River Fault; WMB—Western Mélange Belt; CAN—Canada.

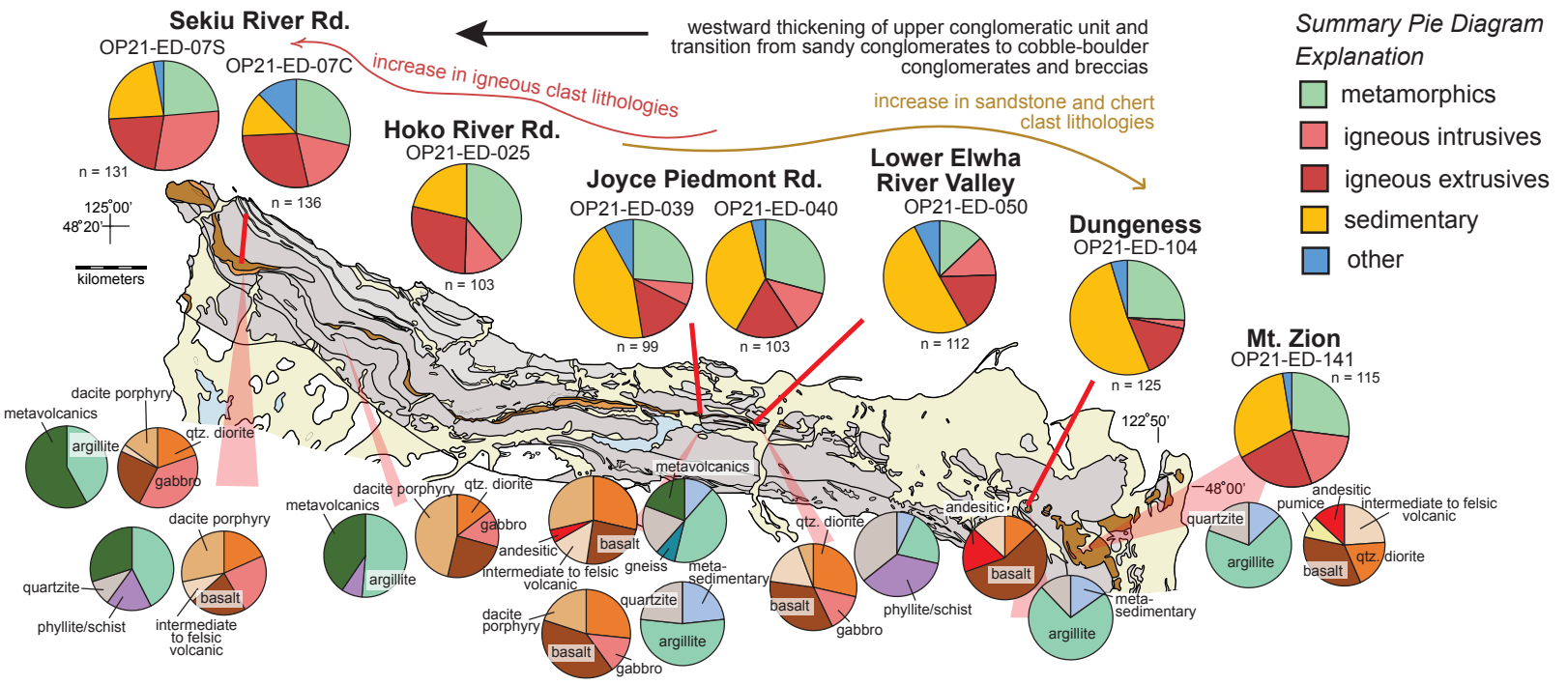

Figure 7. Summary and detailed pie diagrams categorizing conglomerate clast compositions from the Lyre Formation showing along-strike variation in the distribution of conglomerate clast lithologies. Summary pie diagrams show an overall increase in clast lithologies to the west, and an increase in sedimentary clast lithologies to the east. Sedimentary clast lithologies are primarily lithic sandstone and chert (Table SB2, see text footnote 1). Pie diagrams of the igneous and metamorphic detrital mode categories are shown for each location and show more detailed spatial variations in clast compositions. Metavolcanics and gabbro clasts are common in westernmost deposits of the Lyre Formation, whereas there is an increase in basalt, argillite, and intermediate-to-felsic clast lithologies toward the east. qtz.—quartz.

and were interbedded with matrix-supported cobble conglomerate of the Lyre Formation. The andesite andesitic porphyry yields an eruption age of 46.538 ± 0.022 Ma (sample OP21-ED-143), and the adjacent andesite yielded an eruption age of 46.584 ± 048 Ma (sample OP21-ED-141). These ages are slightly younger than the tuff clast dated in the Lyre Formation along Lake Crescent and provide strong evidence that conglomerates in the footwall and hanging wall of the Lower Elwha Fault are temporally correlative. Whole-rock and trace element geochemistry of an andesite sample (sample OP21-ED-143) shows an intermediate composition with enrichment in Al, Na, and light rare earth elements (LREEs) relative to heavy rare earth elements (HREEs; Table SC1).

Postcollisional Hoko River Formation

The Hoko River Formation is ~1600 m thick at its type locality along the Hoko River and overlies the Lyre Formation (Brown and Gower, 1958; Brown and Gower, 1960; Snavely et al., 1977, 1978). We measured stratigraphic sections and completed lithofacies mapping along Hoko River Road, Morse Creek, and the Dungeness Forks area to document changes in depositional environments along strike on the northern Olympic Peninsula (Fig. 2; Figs. SA1, SA3, and SA7). The Hoko River Formation is predominantly thinly bedded siltstone and basaltic sandstone (Fig. 5E; Snavely et al., 1978) and represents a marked change in lithology from the underlying coarse-grained deposits of the Lyre Formation. The contact of the Hoko River Formation with the underlying Lyre Formation is primarily mapped as unconformable, and in some locations, the Hoko River Formation directly overlies Crescent Formation basalts (Fig. 2; Tabor and Cady, 1978a, 1978b; Brown et al., 1956; DeChant, 1989).

Measured stratigraphic sections, coupled with lithofacies mapping along Hoko River Road, indicate that the Hoko River Formation is characterized primarily by thinly bedded, fine-grained deposits of siltstone and lithic-rich sandstone (Fig. SA13). Bedding geometries are generally planar and continuous, and although sedimentary structures are rare, soft sediment deformation is abundant. A high abundance of disarticulated plant fragments and carbonaceous debris is also present in interbedded siltstones and mudstones (Fig. SA13). In the middle Hoko River Formation, numerous volcanic debris flow to hyperconcentrated flow deposits are interbedded with thick sequences of thinly laminated siltstone and claystone. Volcanic debris flow deposits appear silicified, and contain angular, pebble–cobble-sized clasts that are dominantly pumice and silicic tuff and have lenticular bedding geometries. They are generally mapped adjacent to matrix-supported granule–pebble conglomerates with volcanic and lithic clasts (Fig. SA13).

Three sandstone samples were collected in the lower (sample OP20-ED-009), middle (OP20-ED-011), and upper part of the Hoko River Formation (OP20-ED-012) along Hoko River Road to constrain temporal changes in provenance using CA-LA-ICP-MS detrital zircon geochronology. These samples were collected in lithic arenites and graywackes. Samples from the Lower and middle Hoko River Formation have an extremely low abundance of zircon. After processing ~2 kg of rock per sample, ~70–100 zircon grains were recovered from the lower and middle samples. Zircon yield improved marginally for the sandstone in the Upper Hoko River Formation, with ~2 kg of rock yielding ~250–300 zircon grains. All sandstone samples from along the Hoko River yielded a unimodal peak age population of 50–55 Ma (Fig. 6B). Subordinate peak age populations of 65–80 Ma, 80–100 Ma, 155–160 Ma, 170–180 Ma, and 190–210 Ma are present in the Upper Hoko River Formation. These data were supplemented by a sandstone sample (n = 274; sample 092222ED01A) collected from a silicified volcaniclastic sandstone in the Lower–middle Hoko River Formation along Morse Creek in the central part of the northern Olympic Peninsula (Fig. 2). In contrast to western Hoko River Formation sandstones, this sample has a high-zircon yield and more diverse detrital zircon age spectra (500+ zircon grains yielded from ~1 kg of sample; Fig. 6B). Two main peak age populations were identified: 42–52 Ma and 90–100 Ma. Subordinate peak age populations include 70–80 Ma, 100–115 Ma, and 140–165 Ma. To constrain the depositional age of the Hoko River Formation, the four youngest grains were tandem-dated using CA-ID-TIMS to estimate a high-precision MDA. These grains yielded an age of ca. 44 Ma (Table 1), and we believe they are likely representative of the depositional age as they all overlap on concordia, the sample was collected from a sequence with thin interbedded tuffs (DeChant, 1989), and they contained abundant fragments of volcanic glass. This distinct change in provenance relative to other exposures of the Hoko River Formation suggests that a nearby eruptive center supplied the sediment (Table SD1).

One of our biggest changes from previous mapping (Tabor and Cady, 1978a, 1978b; Einarsen, 1987) of the northern Olympic Peninsula is the reclassification of exposures in the Dungeness Forks area as the Hoko River Formation rather than the Blue Mountain Unit (Site 4 in Figs. 2 and 3). At the base of this section, a massive monolithic boulder sedimentary breccia containing columnar basalt clasts is 7–8 m thick (Fig. 5G). Thin interbeds of basaltic sandstone and siltstone overlie this section and contain abundant plant fragments and carbonaceous debris. Strata are also characterized by frequent zones of soft-sediment deformation. Overall, the lithofacies and sandstone composition (enriched in basalt detritus) appear to be very similar to the Hoko River Formation exposed along the Hoko River to the west. This interpretation is not entirely new, as previous researchers (Cady et al., 1972; Tabor and Cady, 1978a, 1978b) also suggested that strata in the Dungeness River area could be part of the peripheral rock sequence.

Postcollisional Makah Formation

The Makah Formation is up to 2800 m thick and is characterized by thin, rhythmic interbeds of fine-grained sandstone and siltstone. Previous researchers mapped the Makah Formation as conformably overlying strata of the Hoko River Formation, with the exception of a local unconformity present in the western Olympic Peninsula in the Hoko River area (Fig. 2; Tabor and Cady, 1978a, 1978b; Snavely et al., 1980; Schasse, 2003). The lowermost Makah Formation

is characterized by lithic- to lithic–feldspathic arenite, but grades up-section to more feldspathic sandstone in the middle to Upper Makah Formation (Fig. 5H; Snavely et al., 1978, 1980; Garver and Brandon, 1994). This marks the first feldspathic sandstone compositions in the peripheral rock strata, as all underlying units are dominantly lithic arenite to graywacke. Additionally, there are seven distinct members mapped within the Makah Formation. These members were not examined in detail in this study, but previous work indicates they are characterized by sequences of massive sandstone, tuff-rich intervals, and olistostromal deposits (Snavely et al., 1980; Garver and Brandon, 1994). The Carpenter Creek Tuff Member in the Lower Makah Formation consists of seven or eight thin, subaqueous, silicified tuffs (Fig. SA14; Snavely et al., 1980; Garver and Brandon, 1994).

We collected one tuff from the Carpenter Creek Tuff Member and another from an unnamed tuff estimated to be ~100 m stratigraphically below by Snavely et al. (1980; Fig. 2). The Carpenter Creek tuff yielded a CA-ID-TIMS eruption age of 31.282 ± 0.069 Ma (sample OP20-ED-014), and the unnamed tuff yielded an eruption age of 31.25 ± 0.13 Ma (OP20-ED-015; Table 1). These sections are separated by a zone of cover along Hoko River Road, and the similarity and overlap in tuff ages suggests either minor fault offset of a similar aged stratigraphic section or that the Carpenter Creek tuff contained reworked zircon from the underlying section. Regardless, these new age data indicate that the lowermost Makah Formation is early Oligocene in age, and suggest that the local unconformity at the base of the Makah Formation developed near the Oligocene–Eocene boundary. Two sandstone samples were also collected in the lower (sample OP20-ED-013) and middle (OP20-ED-016) parts of the Makah Formation along Hoko River Road for CA-LA-ICP-MS detrital zircon geochronology (N = 2; n = 612). The middle sample was collected from a massive sandy member of the Makah Formation (Fig. 5H), and it yielded two major peak age populations of 70–85 Ma and 90–110 Ma. Subordinate peak age populations are 60–70 Ma and 150–160 Ma. The Upper Makah Formation sample yielded a broad range of ages of between 50 Ma and 100 Ma, with the most significant peak age population between 80 Ma and 100 Ma, and subordinate peak age populations of between 140 Ma and 160 Ma (Fig. 6C). Both samples were enriched in zircon relative to the underlying strata, with hundreds of zircons yielded per 1 kg of rock.

SEDIMENTARY RECORD OF STAGES OF SILETZIA OCEANIC PLATEAU COLLISION

Precollisional Basin Development (56–50 Ma): Aldwell Formation

The Aldwell Formation is the lowermost sedimentary unit defined in the northern peripheral rock sequence and immediately overlies Crescent Formation basalts. We interpret discontinuous exposures of massive siltstone and claystone of the Aldwell Formation to represent deep-marine pelagic to hemipelagic sediment accumulation prior to Siletzia's collision with the continental margin at ca. 50 Ma (Fig. 8A). This interpretation is based on new lithofacies mapping (Fig. SA4) and age data from interbedded dacite, volcaniclastic breccia, and a tuff near the base of the Aldwell Formation that are all ca. 52–51 Ma (Table 1). Previous foraminiferal biostratigraphy suggested an early to middle Eocene age (Rau, 1964), which is consistent with our geochronologic data. The types of foraminifera present support deposition at depths of up to ~1500 m, and the Aldwell Formation is inferred to have been deposited by distal deep-water turbidites in a forearc basin (Snavely, 1983; Snavely and Landu, 1983; Rau, 1964). However, these water depths are also common for present-day basins forming on top of oceanic plateaus (Gladczenko and Coffin, 2001), and sandier sections of the Aldwell Formation (e.g., Lake Crescent) likely represent distal turbidite deposits that lapped onto the submerged Siletzia oceanic plateau as it approached the continental margin (Fig. 8A).

Precollisional deposition of the Aldwell Formation helps to explain the variable contact relationships with the underlying Crescent Formation. The contact has been mapped as conformable and interstratified with Crescent basalts (Tabor and Cady, 1978a, 1978b), both unconformable (Snavely, 1983, 1987) and faulted (Schasse, 2003; this study). We hypothesize that deposition and thickness of the Aldwell Formation were controlled by topography on the surface of the plateau prior to accretion. This setting could explain the discontinuous nature of the Aldwell Formation on the northern Olympic Peninsula (Fig. 2). On a ridge-centered plateau such as Siletzia, extensional structures are expected, and Aldwell Formation sediments were likely deposited in grabens and half-grabens adjacent to structurally driven topographic relief (Munschy et al., 1993; Petterson et al., 1997; Davy et al., 2008). Such basins would be isolated, explaining the along-strike changes observed in the Aldwell sandstone petrography and depositional environments, including the discontinuous basal basaltic conglomerate. Although normal faults are uncommon on the northern Olympic Peninsula in the present day, it is likely these structures were reactivated in a compressional regime driven by the collision of Siletzia. Emplacement of ca. 52–51 Ma rhyolites and dacites in only eastern parts of the Aldwell Formation can also be explained within this framework, as local phases of late-stage felsic volcanism have been documented on ancient oceanic plateaus that do not extend across the entire plateau area (Kerr et al., 1996; White et al., 1999; Frey et al., 2000).

It is important to note that these felsic to intermediate volcanics and their relationships to the Aldwell Formation have been debated. Some previous researchers mapped these volcanics as interbedded with the lowermost Aldwell Formation on the north-central part of the Olympic Peninsula (Tabor and Cady, 1978a, 1978b). In contrast, Snavely (1983) mapped them as isolated lenses of volcanic conglomerate, breccia, and large olistostrome blocks derived from Striped Peak (Fig. 2). Mapping the lithofacies and structure of the central part of the northern Olympic Peninsula helped to constrain the debated depositional history of the lowermost Aldwell Formation and intermediate to felsic volcanics. The interbedded dacite in the Dry Hills represents a flow proximal to an eruptive vent based on interfingering sequences of volcanic conglomerate, breccias, rhyolite to dacite flows, and massive sections of mudstone. Two

A. 52-50 Ma - Deposition of the Precollision Aldwell Fm.

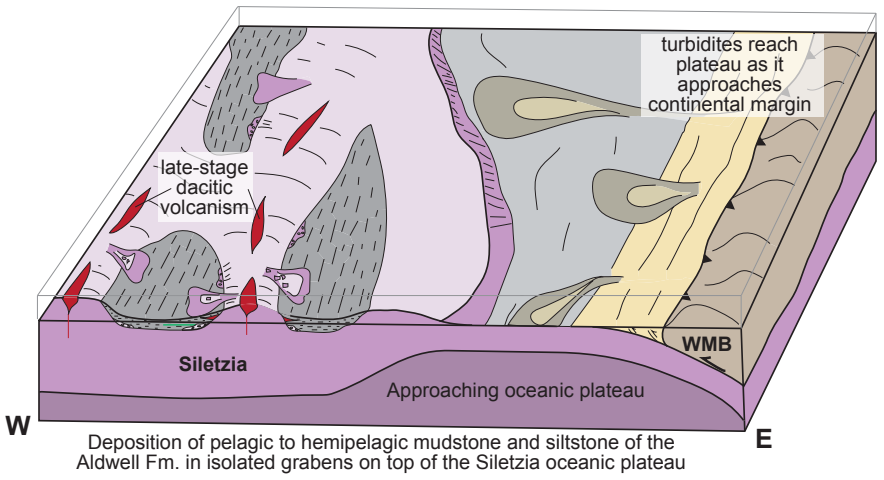

Deposition of pelagic to hemipelagic mudstone and siltstone of the Aldwell Fm. in isolated grabens on top of the Siletzia oceanic plateau

B. 48-46.5 Ma - Syn-collisional deposits of the Lyre Fm.

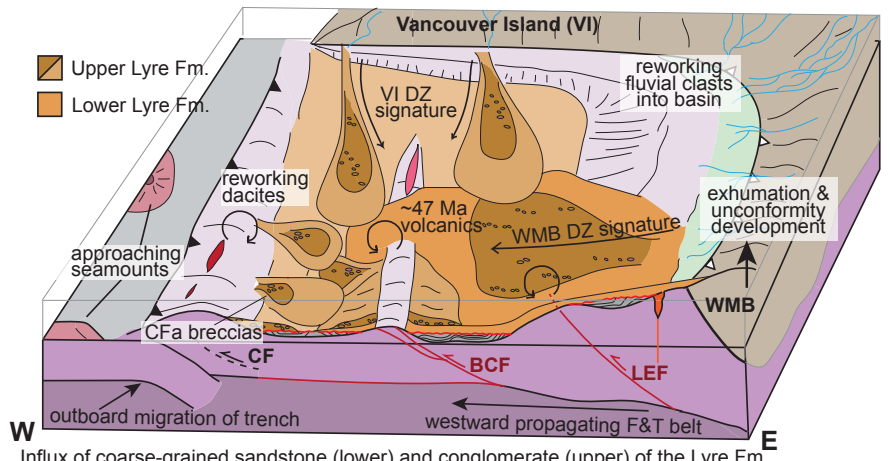

Influx of coarse-grained sandstone (lower) and conglomerate (upper) of the Lyre Fm. following collision of the Siletzia plateau. Deformation of pre-accretion sequence leads to unconformity development and reworking of lower Lyre, Aldwell, and Crescent Fms.

C. 45-35 Ma - Hoko River Fm. deposition in isolated (lower) to integrated (upper) trench-slope basins

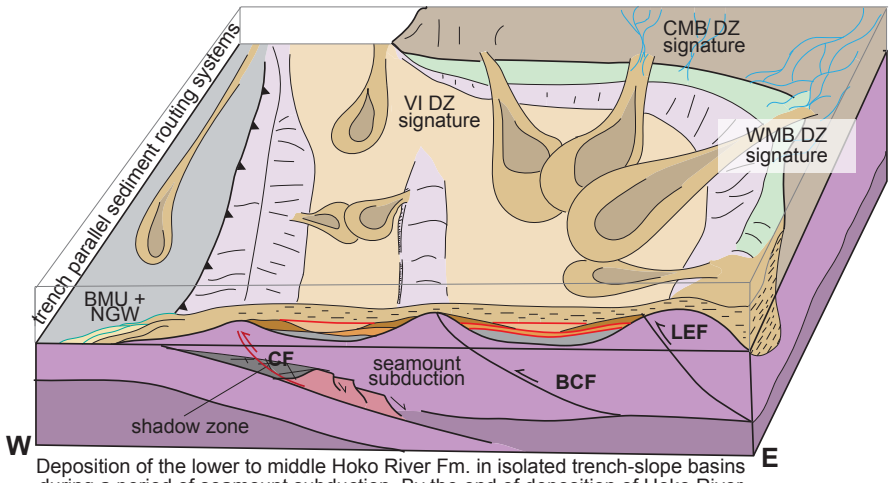

Deposition of the lower to middle Hoko River Fm. in isolated trench-slope basins during a period of seamount subduction. By the end of deposition of Hoko River Fm., sediments derived from the continent overtopped topographic highs to form a regional forearc basin.

D. 35-25 Ma - Makah Fm. marks transition from trench-slope to Regional Tofino-Juan de Fuca basin

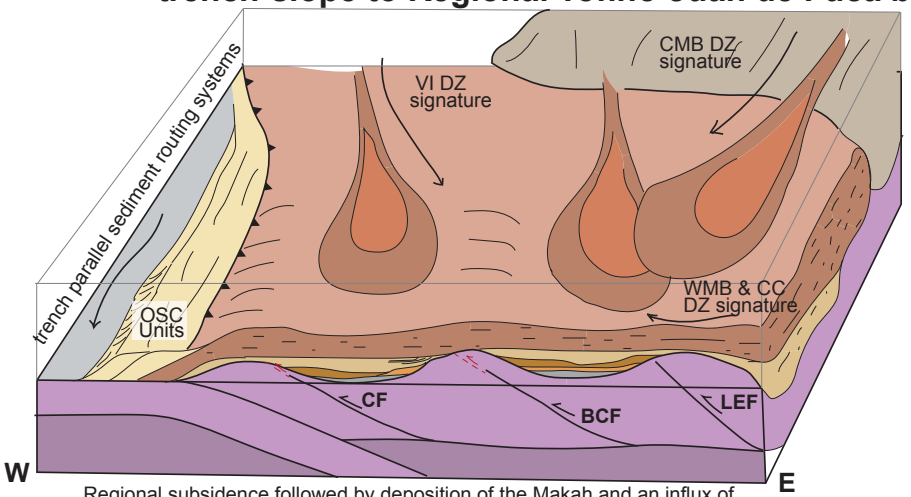

Regional subsidence followed by deposition of the Makah and an influx of continentally-derived sediment and development of the regional Tofino-Juan de Fuca forearc basin.

Figure 8. (A) Massive mudstone and siltstone of the Aldwell Formation represents precollisional pelagic to hemipelagic basin deposits in isolated grabens on the Siletzia terrane. Interbedded sandstone in the Aldwell Formation represents turbidity currents that reached the plateau as it approached the continental margin prior to collision. Interbedded volcaniclastic conglomerate, breccia, tuff, and intermediate to felsic volcanics in the Lower Aldwell Formation support late-stage silicic volcanism during end-phases of oceanic plateau construction. (B) Collision of Siletzia resulted in an influx of coarse-grained sediment onto the accreted fragment of oceanic plateau; an angular unconformity marks this collision and separates the lower sandy member of the Lyre Formation from underlying deformed Aldwell and Crescent Formation rocks. Deformation was the result of a westward-propagating fold-and-thrust belt onto the accreted fragment of Siletzia; the lower sandy member of the Lyre Formation represents initial sheet sands and distal turbidite deposits derived from continental sources delivered to the newly formed basin on top of Siletzia. Outboard migration of the trench occurred by ca. 48 Ma, and this resulted in exhumation near the trench and deposition of Cape Flattery breccias. The accreted fragment of Siletzia was incorporated into the new subduction complex following outboard trench migration. Continued exhumation along the Lower Elwha Fault (LEF) and Boundary Creek Fault (BCF) in the subduction complex reworked precollisional units into isolated trench-slope basins as the conglomeratic upper member of the Lyre Formation. This is mixed with continued deposition of continentally derived sediments. (C) The postcollisional phase of basin deposition is marked by the Hoko River Formation. Seamount subduction results in exhumation of the frontal subduction complex and an influx of basaltic detritus from exhumed basement basalt material into isolated trench-slope basins. Most of the Hoko River Formation is characterized by distal deep-marine turbidite deposits and marks a period of regional subsidence following seamount subduction. This results in an infilling of isolated trench-slope basins and a more integrated regional basin through deposition of the Upper Hoko River Formation. (D) Continued subsidence and an influx of continentally derived sediment results in the establishment of the regional Tofino–Juan de Fuca forearc basin. Compositional and geochronologic data support a strong influence from continentally derived sources further inboard than the Western Mélange Belt (WMB), such as the Coast Mountains Batholith (CMB) and Cascades Crystalline Core (CC). Age and composition of the Makah Formation correlate to the Carmanah Group on southern Vancouver Island (VI), and further support a more integrated and regional forearc basin system at this time. Local faulting, unconformity development, and broad regional folding of the Hoko River and Makah formations indicate that regional faults likely remained active during the Oligocene. BMU—Blue Mountain Unit; CF—Crescent Fault; CFa—Cape Flattery; DZ—detrital zircon; NGW—Needles–Gray Wolf Lithic Assemblage; OSC—Olympic subduction complex.

conglomerate clasts dated from the volcanic breccia in the Lower Elwha area and a tuff from the Lake Crescent area (Fig. 2) yielded similar ages relative to the massive dacite in the Dry Hills (Table 1). This change in the Lower Aldwell Formation from massive flows of dacite in the Dry Hills to thin tuffs at Lake Crescent records proximal to distal lithofacies associated with a felsic volcanic center (Fig. SA4). This type of volcanism can be associated with the end stages of oceanic plateau construction, and whole-rock geochemical data from the dacite is consistent with an origin via partial melting of a hydrous basaltic source (Table SC1; Kerr et al., 1996; Frey et al., 2000; Wanless et al., 2010).

Along-strike variations in compositional provenance data of the Aldwell Formation also support deposition in isolated preaccretion basins. Although we targeted the Aldwell Formation for detrital zircon analyses in sandier sections of the Dry Hills and along the Sekiu River (Fig. 2), we reinterpreted both sections as the lowermost sandy member of the Lyre Formation (Site 3 in Figs. 2 and 3). This reinterpretation is not surprising, as the Aldwell Formation is dominated by massive sections of fractured mudstone (Figs. 5A and 5B), consistent with its hemipelagic to pelagic nature in most locations. Additionally, this interpretation is supported by previous mapping of the Lower Lyre Formation in the Dry Hills (Polenz et al., 2004) and Sekiu River (Brown et al., 1956; Ansfield, 1972), as well as rare 49–46 Ma detrital zircon present in our samples (Fig. 6). Previous petrographic studies of sandstone document western Aldwell Formation lithic arenites that consist primarily of radiolarian chert and argillite lithic fragments, whereas eastern Aldwell Formation sandstone compositions shift to lithic graywackes with primarily basalt lithic fragments (Marcott, 1984). Both basaltic and chert-rich sediments of the Aldwell Formation were thought to be derived from southern Vancouver Island, specifically the Metchosin and Leech River complexes (Marcott, 1984). The Metchosin Complex is a partial ophiolitic sequence characterized by gabbros, sheeted dikes, quartz diorite, plagiogranite, and basalt flows (Massey, 1986). It has been correlated to the Crescent Formation, Bremerton Complex, and the Black Hills basalts based on timing of emplacement (Eddy et al., 2017). However, it is unlikely that these sources supplied sediment to the Aldwell Formation, because the Metchosin Complex was built contemporaneously with deposition of the Aldwell Formation and the Leech River Complex was not uplifted and exposed until after Siletzia's accretion (Clowes et al., 1987; Massey, 1986; Wanless et al., 1978; Fairchild and Cowan, 1982; Seyler et al., 2021). Instead, we suggest that chert- and basalt-rich detritus of the Aldwell Formation could have been locally sourced from sources on and immediately adjacent to Siletzia, with minor distal turbidite input from continentally derived sources (Fig. 8A).

It is common to have thick sedimentary deposits on top of oceanic plateaus, although they are frequently pelagic to hemipelagic in nature (Davy et al., 2008; Jovane et al., 2016). The silty nature and hemipelagic muds of the Aldwell Formation support its deposition as deep-marine distal deposits with only minor influx from continentally derived sediments (Fig. 8A). Previous research on the Ontong-Java plateau documents a transition from dominantly pelagic and hemipelagic sediments (1–2 km) to arc-derived turbidites as the oceanic plateau approached the Solomon Arc (Faugères et al., 1989; Petterson et al., 1997). This is comparable to along-strike lithofacies and compositional variations in the Aldwell Formation, where eastern and western exposures have variable compositional provenance signatures and distributions of sandstone. These differences may reflect which part of the Aldwell Formation is exposed (lower versus upper), as well as spatial variation in preaccretion proximity to the continental margin. Furthermore, the overall proximity of Siletzia to the continent as it formed may have allowed for more continentally derived turbidites to reach the basin early in its history as it approached the margin.

Syn-Collision to Postcollision (50–45 Ma): Lyre Formation

The Lyre Formation is subdivided into a lower sandy member and an upper conglomeratic member, with both units mapped as discontinuous exposures across the northern Olympic Peninsula (Tabor and Cady, 1978a, 1978b; Ansfield, 1972; Brown et al., 1956). The contact with the underlying Aldwell Formation is rarely observed, but north of the Boundary Creek Fault, the sandy lower member of the Lyre Formation is separated from preaccretion Aldwell Formation mudstones (ca. 52–51 Ma) by an angular unconformity (Fig. 4D). West of Lake Crescent, the contact was described as gradational in the Lyre and Sekiu River areas, and the lack of the lower member was due to nondeposition (Brown et al., 1956). New geochronologic data from interbedded andesites and tuff breccia within the Lyre Formation yielded ages of ca. 46.5–47 Ma (Table 1), and we interpret massive sandstone, sandy conglomerate, boulder–cobble conglomerate and breccia of the Lyre Formation to represent syn-collisional and postcollisional submarine channel-fill and debris-flow deposits related to the collision and accretion of Siletzia. Collision of the Siletzia terrane with the continental margin resulted in exhumation and deformation of the preaccretion Aldwell and Crescent formations into a west-verging fold-and-thrust belt prior to the influx of coarse-grained Lyre Formation material onto the accreted Siletzia plateau (Fig. 8B).

Evidence for a west-verging fold-and-thrust belt propagating onto Siletzia and deforming precollisional units is present in both surface and subsurface data. In the subsurface, duplexing and imbrication of Siletzia basement basalts is evident on seismic lines taken offshore of Vancouver Island in the Tofino basin (Spence et al., 1991), and from new geophysical studies over the Seattle uplift that document the duplication of Crescent Formation basalts in imbricate thrust sheets beneath the Western Mélange Belt (Anderson et al., 2024). Surface geology on the northern Olympic Peninsula is also consistent with imbrication and duplexing of the Crescent Formation along the Lower Elwha Fault and Boundary Creek Fault (Figs. 9A and 9B). These two faults separate peripheral sedimentary strata, underlying Crescent Formation basalt, and Olympic subduction complex rocks into distinct structural blocks (Fig. 3). While these structures undoubtedly were reactivated during later Oligocene–Miocene events (Brandon and Calderwood, 1990; Brandon and Vance, 1992a, 1992b; Shekut and Licht, 2020), the discontinuous map patterns; repetition of lower units; and folds that are isolated to the Crescent, Aldwell, and Lyre formations

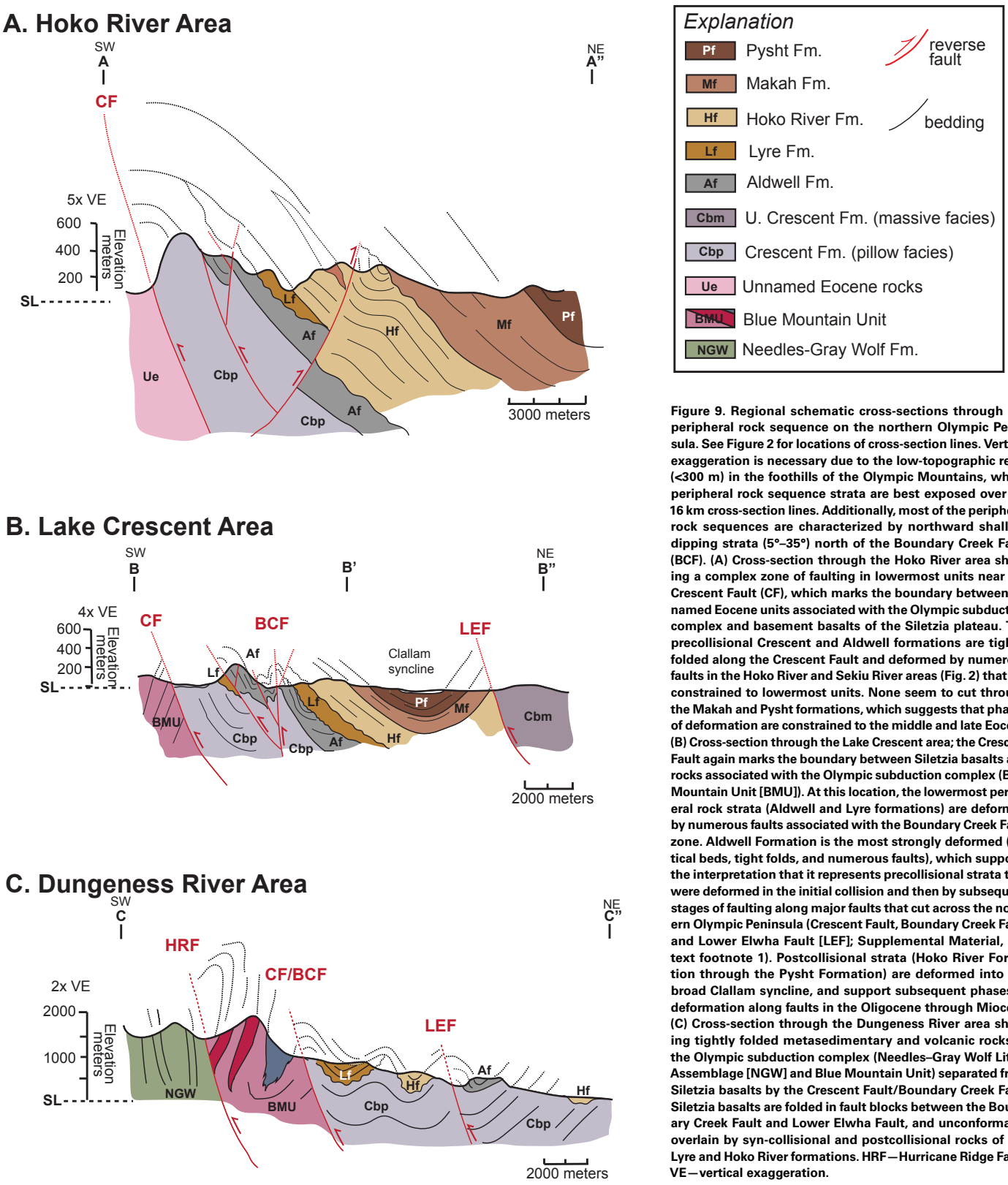

Figure 9. Regional schematic cross-sections through the peripheral rock sequence on the northern Olympic Peninsula. See Figure 2 for locations of cross-section lines. Vertical exaggeration is necessary due to the low-topographic relief (<300 m) in the foothills of the Olympic Mountains, where peripheral rock sequence strata are best exposed over 15–16 km cross-section lines. Additionally, most of the peripheral rock sequences are characterized by northward shallow-dipping strata (5°–35°) north of the Boundary Creek Fault (BCF). (A) Cross-section through the Hoko River area showing a complex zone of faulting in lowermost units near the Crescent Fault (CF), which marks the boundary between unnamed Eocene units associated with the Olympic subduction complex and basement basalts of the Siletzia plateau. The precollisional Crescent and Aldwell formations are tightly folded along the Crescent Fault and deformed by numerous faults in the Hoko River and Sekiu River areas (Fig. 2) that are constrained to lowermost units. None seem to cut through the Makah and Pysht formations, which suggests that phases of deformation are constrained to the middle and late Eocene. (B) Cross-section through the Lake Crescent area; the Crescent Fault again marks the boundary between Siletzia basalts and rocks associated with the Olympic subduction complex (Blue Mountain Unit [BMU]). At this location, the lowermost peripheral rock strata (Aldwell and Lyre formations) are deformed by numerous faults associated with the Boundary Creek Fault zone. Aldwell Formation is the most strongly deformed (vertical beds, tight folds, and numerous faults), which supports the interpretation that it represents precollisional strata that were deformed in the initial collision and then by subsequent stages of faulting along major faults that cut across the northern Olympic Peninsula (Crescent Fault, Boundary Creek Fault, and Lower Elwha Fault [LEF]; Supplemental Material, see text footnote 1). Postcollisional strata (Hoko River Formation through the Pysht Formation) are deformed into the broad Clallam syncline, and support subsequent phases of deformation along faults in the Oligocene through Miocene. (C) Cross-section through the Dungeness River area showing tightly folded metasedimentary and volcanic rocks of the Olympic subduction complex (Needles–Gray Wolf Lithic Assemblage [NGW] and Blue Mountain Unit) separated from Siletzia basalts by the Crescent Fault/Boundary Creek Fault. Siletzia basalts are folded in fault blocks between the Boundary Creek Fault and Lower Elwha Fault, and unconformably overlain by syn-collisional and postcollisional rocks of the Lyre and Hoko River formations. HRF—Hurricane Ridge Fault; VE—vertical exaggeration.

suggest that these faults were active in the Eocene (Fig. 9B; McWilliams, 1970; MacLeod et al., 1977; Snavely, 1983).

Due to the erosional lower contact of the upper conglomeratic member, the thickness of the lower sandy member of the Lyre Formation and underlying Aldwell Formation vary greatly along strike (Fig. 2). This variability has made it difficult to understand their depositional and structural relationships. Where the contact is observed north of Lake Crescent, an angular unconformity separates the lower sandy member of the Lyre Formation from underlying preaccretion mudstones of the Aldwell Formation (Fig. 4D). Elsewhere, the lower sandy member of the Lyre Formation is entirely absent, and the upper conglomeratic member overlies either the Aldwell or Crescent Formation. This suggests the boundary between the upper and lower Lyre members is also marked by a regional unconformity and represents a period of tectonic faulting (McWilliams, 1970). We interpret the Lyre Formation to have been deposited on an actively deforming landscape based on slumped to overturned bedding and large olistostromal to mass-transport deposits. Tectonic drivers, such as fold-and-thrust belt development, also result in the onlapping of conglomeratic units on underlying basin-fill or basement rock (Massari and Colella, 1988) and match the outcrop pattern and contact relations of the Lyre Formation with underlying units (Tabor and Cady, 1978a, 1978b; Snavely et al., 1986). These conglomeratic deposits often represent nearby cannibalized alluvial fans, deltas, or nearshore materials in forearc settings and are the result of relative sea-level fall (Massari and Colella, 1988), and help to explain the abundance of rounded to subrounded cobble conglomerate clasts of the Lyre Formation (Fig. 8B).

Geochronologic and compositional data also show distinct differences in provenance between the lower and upper members of the Lyre Formation. Detrital zircon age spectra from the lower sandy member of the Lyre Formation on the central-eastern part of the Olympic Peninsula have distinct 60–70 Ma, 80–90 Ma, 100–130 Ma, and 150–180 Ma peak age populations (Fig. 6A). On the western Olympic Peninsula, age-equivalent strata have detrital zircon spectra similar to those in the east but without the 50–100 Ma age populations (Fig. 6A). Detrital zircon spectra from the upper conglomeratic member are broadly similar to those of the underlying sandy member but with an increased abundance of 50–56 Ma ages. We will discuss the significance of this change in the next paragraph. The 70–75 Ma, 90 Ma, 110 Ma, and 160–180 Ma age populations in the Lyre Formation are common in the Western Mélange Belt (Sauer et al., 2017, 2018), which served as the backstop to Siletzia's collision in Washington (Fig. 8B). The Western Mélange Belt is an accretionary complex that is characterized by argillite, sandstone, chert, marble, metagabbro, and metadiabase (Jett and Heller, 1988; Tabor et al., 1989; Dragovich et al., 2009), which all are clast types commonly found in the upper conglomeratic member of the Lyre Formation (Fig. 7). The 90–100 Ma and 100–140 Ma peak ages can also be associated with felsic to intermediate igneous intrusions in the Coast Mountains Batholith and Cascades crystalline core, but these sources seem unlikely to be a primary contributor of detritus because these source lithologies are uncommon in conglomerate clast compositions (Figs. 6 and 7).

The greatest change in the detrital zircon age spectra between the lower and upper members of the Lyre Formation is the prominent increase in the 52 Ma peak age population in the upper conglomerate member on the western Olympic Peninsula. This also coincides with a large proportion of dacite porphyry and green metavolcanic conglomerate clasts in the Cape Flattery breccia (Ansfield, 1972; Shilhanek, 1992) and western conglomerates (Fig. 7). The most proximal source for the 48–52 Ma ages is the ca. 52–51 Ma dacites interbedded in the Lower Aldwell Formation. More distal sources are the dacitic to rhyolitic Clayoquot volcanics on the southern tip of Vancouver Island (Madsen et al., 2006). We prefer a proximal source region based on the coarse-grained nature and angular clasts of the breccias. However, interbedded dacite flows are not mapped in the Aldwell Formation on the western Olympic Peninsula, which suggests that any proximal source was fully exhumed and eroded (Fig. 8B). Notably, this period overlaps with a broader phase of near-trench volcanism between 51 Ma and 47 Ma in western Washington (Irving and Brandon, 1990; Tepper et al., 2004; Madsen et al., 2006; Eddy et al., 2016; Kant et al., 2018) and 46.5–46.9 Ma andesitic adakitic volcanism within the Upper Lyre Formation (Tepper and Clark, 2024). The presence of intermediate to felsic tuff clasts in all Lyre conglomerate beds supports synchronous derivation of interbedded volcanics during deposition (Fig. 7). For example, the meters-wide ca. 47 Ma intermediate to felsic tuff clasts at Lake Crescent in the breccia must have been deposited proximal to the source. However, no ca. 47 Ma thick-bedded tuffs have been mapped on the northern Olympic Peninsula, which indicates another setting where conglomerate and breccia were deposited proximal to sources that have been exhumed and completely eroded (Fig. 8B).

The collision of Siletzia is marked by the deformation of all underlying preaccretion units (Crescent and Aldwell formations) into imbricate thrust sheets (Fig. 9) and the development of regional unconformity prior to deposition of the Lyre Formation outboard of the suture (Fig. 8B). Possible paleosol development along the surface of the unconformity suggests that parts of the plateau could have been subaerially exposed during collision, especially in eastern exposures more proximal to the suture. Initial syn-collisional sediments are marked by the lower sandy member of the Lyre Formation, which derived sediments primarily from the exhumed Western Mélange Belt and reworking of underlying preaccretion units (Fig. 8B). Interbedded sandstone, siltstone, and sandy conglomerate of the lower sandstone member of the Lyre Formation represent deposition by turbidity currents and debris flows on a submarine fan that prograded out on top of accreted fragments of Siletzia (Fig. SA12). Topography created during exhumation of the Western Mélange Belt separated the previous Paleocene–Eocene forearc region from the new Eocene forearc and trench-slope areas. We think that outboard migration of the trench west of Siletzia is marked by the unconformity that separates the lower sandy member from the upper conglomeratic member of the Lyre Formation. The conglomeratic upper member of the Lyre Formation was deposited in structurally controlled valleys within the new forearc region defined by both preexisting plateau topography and the developing collisional fold-and-thrust belt (Fig. 8B). Conglomerate beds represent channel and debris flow deposits

on proximal submarine fans adjacent to structural highlands that reworked the sandy lower member of the Lyre, Aldwell, and Crescent formations (Fig. 8B). Although the lack of the lower sandy member can also be partly related to nondeposition in the distal parts of the basin (Brown et al., 1956), erosion by the upper member helps to explain its discontinuous nature across the entire northern Olympic Peninsula. Continentally derived detritus from the Western Mélange Belt was likely reworked from nearshore deltaic to fluvial deposits as mass-transport deposits and helps to explain the rounding of conglomerate clasts in the Lyre Formation and matrix-supported fabrics. Interbedded ca. 46.5–47 Ma andesites in the upper conglomeratic member of the Lyre Formation have an adakitic geochemical affinity (Table SC1) and support the melting of subducted oceanic crust. This process could happen along slab edges, or in the presence of a slab tear or window beneath the actively accreting Siletzia plateau (Thorkelson and Taylor, 1989; Ickert et al., 2009; Tepper and Clark, 2024; Tepper et al., 2024; Anderson et al., 2024).

Postcollisional Deposition in Trench-Slope Basins (45–35 Ma): Hoko River Formation

Following the accretion of Siletzia, thicker and more regionally continuous strata of the Hoko River Formation were deposited across the northern Olympic Peninsula (Fig. 2). The Hoko River Formation unconformably overlies the Lyre and Aldwell formations, and at some locations it even sits directly on top of Crescent basalts (Tabor and Cady, 1978a, 1978b). This unconformity is thought to represent a major tectonic event marked by an influx of basaltic detritus into the basin (Brown et al., 1956). The overall fine-grained nature of the Hoko River Formation is also a stark contrast to the underlying conglomeratic unit of the Lyre Formation, and indicates a rapid shift in depositional environments from proximal mass transport and submarine channel deposits of the Lyre Formation to distal and medial submarine fan deposits of the Hoko River Formation. This increased accommodation space could be associated with the initial stages of thermal subsidence of the Siletzia oceanic plateau following the accretion and outboard migration of the subduction zone (Laursen et al., 2002; Patriat et al., 2019). The location of the Hoko River Formation and proximity to the trench in the overall forearc geometry suggest deposition in trench-slope basins on top of the accreted imbricated slivers of Siletzia basalt (Fig 8C).

The Hoko River Formation is estimated to be middle to late Eocene in age based on our new age data, and previously foraminifera and mollusk fossils were documented (Rau, 1964; Mallory, 1959). It was deposited by turbidity currents on the medial to distal parts of a submarine fan system (Snavely et al., 1978; Snavely, 1987; DeChant, 1989). Lithic-rich massive to thinly bedded sandstone and siltstone frequently contain zones of convolute bedding and soft sediment deformation (Fig 5F; Rau, 1964; Mallory, 1959; Snavely et al., 1977). Locally exposed matrix-supported conglomerates, with clasts of basalt ranging to boulder sized, represent mass transport deposits and suggest that the Hoko River Formation was deposited during a period active slumping and sliding on the trench-slope (Fig. 8). However, these conglomerate beds are rare in the Hoko River Formation, and comprise <5% of total lithofacies (Fig. SA13). Sandstone compositions and conglomerate clast lithologies are dominated by basalt, and support the interpretation that following the development of unconformity (Brown et al., 1956), deposition of the Hoko River Formation corresponded to an influx of basalt detritus to the basin.

Detrital zircon age spectra vary drastically between the western and eastern exposures of the Hoko River Formation (Fig. 6B), but overall they support reworking of the underlying Crescent basalts. Along Morse Creek in the Lower to middle Hoko River Formation (Fig. 2), there are two young peak age populations of 44–46 Ma and 50–52 Ma (Fig. 6B). This sample was collected from a volcaniclastic sandstone exposed in a section enriched in volcanic glass and interbedded with kaolinized tuffs (e.g., DeChant, 1989). Due to the high proportions of volcanics at this location, it is thought that the strata were deposited proximal to an eruptive center. Thus, we consider our ca. 45 Ma MDA (Table 1) to approximate the depositional age. In addition to the 50–52 Ma peak age population that matches the age of the underlying Crescent Formation, peak age populations of 70–80 Ma, 90–120 Ma, and 150–200 Ma match the ages of source terranes present at southern Vancouver Island (Wrangellia and Nanaimo groups), the Western Mélange Belt, and the southern Coast Mountains Batholith (Fig. 6; Matthews et al., 2017; Cecil et al., 2018; Coutts et al., 2020; Sauer et al., 2017, 2018). These detrital zircon age spectra are identical to a sandstone sample collected in what was previously mapped as the Blue Mountain Unit along the Dungeness River (Eddy et al., 2017; Einarsen, 1987) and provide further evidence that strata at that location belong to the Hoko River Formation (Fig. 3). Furthermore, Cretaceous detrital zircons indicate that either detritus derived from the continent was making it to the easternmost basin deposits of the Hoko River Formation, or there was reworking of the underlying Lyre Formation based on similar detrital zircon age populations and sedimentary lithics (DeChant, 1989) at this location (Fig. 8C).

On the western Olympic Peninsula, the Lower Hoko River Formation detrital zircon age spectra are characterized by a unimodal peak age population of 50–56 Ma that matches the age of the underlying basaltic/gabbroic basement and silicic magmas of Siletzia and nearby near-trench intrusions (Fig. 6B). This unimodal peak age population is prevalent in sandstone samples collected in the middle and upper parts of the Hoko River Formation at this location. Sandstone samples were enriched in basalt detritus, and had extremely low-zircon abundance, which supports derivation from primarily basaltic sources. The minor presence of 60–100 Ma and 150–200 Ma peak age populations in the Upper Hoko River Formation suggests that by the time the Upper Hoko River Formation was deposited, sediments derived from continental sources were finally making their way out to more distal trench-slope basins that represent westernmost deposits of the Hoko River Formation (Fig. 8C). This interpretation is preferred to reworking of the Lyre Formation due to the rarity of >52 Ma detrital zircons and lack of sedimentary lithics.

Outboard migration of the trench resulted in fragments of the newly accreted Siletzia plateau being incorporated into the actively forming

subduction complex (Fig. 8C). Fold-and-thrust belt deformation on the frontal portion of this subduction complex created new topographic highs that resulted in isolated basins on the trench-slope during deposition of the Lower and middle Hoko River Formation (Fig. 8C). Deformation on the frontal part of the accretionary wedge can occur during the subduction of seamounts (Laursen et al., 2002; Festa et al., 2022; Yang et al., 2022), which are commonly found adjacent to spreading ridges and oceanic plateaus (Faugères et al., 1989; Davy et al., 2008) or as a result of continued plate convergence. We prefer a seamount subduction model because the subduction of these features results in exhumation of the frontal wedge and instability on the trench-slope (Festa et al., 2022; Yang et al., 2022) and helps to explain the development of unconformity between deposition of the Lyre and Hoko River formations. Slump deposits and boulder conglomerate (debris flows and olistostromes) with primarily basaltic clasts in the Hoko River Formation indicate a period of instability as detritus slid into the basin adjacent to topographic highs. With continued subsidence following seamount subduction, a more regionally extensive trench-slope to forearc basin was developed as sediments were able to overtop structural highs and detritus from continental sources finally started to make its way to trench-slope basins on the outer wedge (Fig. 8C). Additionally, interbedded volcanic debris flows in the Lower to middle Hoko River Formation remain undated, but could correlate to a phase of volcanism tied to the establishment of the ancestral Cascadia arc at this time. Based on the ca. 45 Ma MDA for the Lower Hoko River Formation, this phase of volcanism must be this age or younger.

Trench-Slope to Forearc Basin Transition (35–28[?] Ma): Makah Formation

The Makah Formation is the first unit in the peripheral rock sequence that marks a transition from local deposition of lithic graywacke and arenite to predominantly continentally derived feldspathic and arkosic arenite (Snavely et al., 1978, 1980; Garver and Brandon, 1994). The Makah Formation is regionally extensive across the northern Olympic Peninsula. It has seven distinct members (Snavely et al., 1980; Garver and Brandon, 1994), and a local angular unconformity separates folded and faulted strata of the Upper Hoko River Formation from the Makah Formation along the western Olympic Peninsula (Fig. 2). Overall, the unit is characterized by thin, rhythmic interbeds of fine-grained sandstone and siltstone that are interpreted to have been deposited on medial to distal reaches of a submarine fan system (Tabor and Cady, 1978a, 1978b; Snavely et al., 1977; Durham, 1944; Brown and Gower, 1958). Based on foraminifera and mollusk fossils, the age of the Makah Formation is estimated to be late Eocene to Oligocene (Rau, 1964). This agrees with our eruption age for the Carpenter Creek tuff (31.282 ± 0.069 Ma) and the underlying unnamed tuff (31.13 ± 0.13 Ma; Table 1). This puts the Eocene–Oligocene boundary in the lowermost part of the Makah Formation or possibly during the development of a local unconformity that separates the Makah Formation from the underlying Hoko River Formation (Fig. 3; Rau, 1964; Tabor and Cady, 1978a, 1978b; Snavely et al., 1980; Schasse, 2003). Continued regional subsidence through the Oligocene allowed for the establishment of an extensive forearc basin during deposition of the Makah Formation.

Detrital zircon age spectra from sandstone samples collected from the middle and Upper Makah Formation along the Hoko River support sediment derivation from continental sources during this time. Peak age populations of between 50 Ma and 100 Ma and between 140 Ma and 160 Ma (Fig. 6C) are consistent with derivation from reworking of the Nanaimo Group and Wrangellia terranes, as well as derivation from the southern part of the Coast Mountains Batholith and central Washington. Additionally, detrital zircon age groups are similar to those found in the Lyre Formation, but lack the 50–52 Ma ages that are dominant in both the underlying lithic-rich Hoko River and Upper Lyre formations (Fig. 6). The Hoko River Formation is also regionally continuous. If detrital zircon from the Lyre and Hoko River formations were recycled into the Makah formation, we would expect a greater proportion of 50–52 Ma ages and lithic fragments in Makah formation sandstones. We also would expect indications of exhumation of the underlying sequence, such as development of a major unconformity and/or areas missing parts or all of these units. Sediment routing systems more likely derived sediments from northeasterly and easterly sources in southern British Columbia (Coast Mountains Batholith), Vancouver Island (Nanaimo Group and Wrangellia), and central Washington sources (Eastern and Western Mélange belts and Central Washington Cascades), consistent with more quartz- and feldspathic-rich sandstone compositions.

The continued thermal subsidence of Siletzia created the accommodation space necessary for the regional Tofino–Juan de Fuca forearc basin. The Oligocene Escalante and Hesquiat formations of the Carmanah Group on southern Vancouver Island are age-equivalent to the thick Makah Formation (Snavely et al., 1980; Garver and Brandon, 1994), and limited well and seismic data suggest that these formations prograded out across the Strait of Juan de Fuca and along the western coast of Vancouver Island (Fig. 1; Spence et al., 1991). Makah sediments were primarily derived from continental sources in southern British Columbia, Vancouver Island, and central Washington, likely by southwestward- and westward-flowing rivers across low-lying Mélange Group rocks and Vancouver Island. There was also transport of sediment from more distal parts of the central Coast Mountains Batholith (Bella Coola area) in the Tofino basin along the western coast of Vancouver Island, based on compositional and geochronologic data (Garver and Brandon, 1994; Parrish, 1983; Snavely et al., 1980). Sediment provenance data provide strong evidence that by the time of deposition of the Makah Formation, a transition had occurred from isolated trench-slope basins to a well-established forearc basin system with both along-axis and transverse basin sediment-routing systems (Fig. 8D). These forearc basin deposits likely represent the distal portion of a broader forearc region due to their location overtopping the subduction complex, and the presence of extensive age-equivalent Eocene (Puget Group; White, 1888; Wolfe et al., 1961) and Oligocene sedimentary rocks (Lincoln Creek Formation; Weaver, 1912; Beikman et al., 1967) located to the east and southeast. Broad

regional folding, faulting, and unconformity development within late Eocene to Oligocene units indicate that structures in the northern Olympic Peninsula remained active, with minor offset through the Oligocene. These characteristics are consistent with fold-thrust deformation mechanisms on the outer wedge of an active subduction complex (Fig. 2; Laursen et al., 2002; Festa et al., 2022). Later Miocene deformation associated with the exhumation of the Olympic Mountains (Brandon and Calderwood, 1990; Brandon and Vance, 1992a, 1992b) likely reactivated and rotated major structures on the Olympic Peninsula to vertical during development of the orocline, helping to explain the minor deformation observed in the Makah Formation (Fig. 1).

GENERALIZED SEDIMENTARY RECORD OF YOUNG OCEANIC PLATEAU COLLISIONS

Eocene–Oligocene sedimentary strata of the northern peripheral rock sequence on the Olympic Peninsula record the collision of a young oceanic plateau (Fig. 10). Additionally, because the Siletzia plateau extends for over 800 km from Vancouver Island to Oregon, we can broadly compare the sedimentary response along different parts of the margin. In northern Washington, the thinner, younger edge of the Siletzia plateau interacted with the continental margin (Trehu et al., 1994) and resulted in the imbrication of basement basalts beneath the Western Mélange Belt, which served as the backstop to collision (Anderson et al., 2024). The Western Mélange fold-and-thrust belt propagated westward onto the accreted portion of Siletzia and was coeval with an influx of sandy debris flows and sheet sands of the Lower Lyre Formation that unconformably overlie preaccretion siltstones of the Aldwell Formation and Siletzia basalts (Crescent Formation). Where the older, thicker portion of the Siletzia plateau collided with Oregon, we observed a similar sedimentary response. During collision, Mesozoic accretionary prism rocks were thrust over Siletzia basalts near Roseburg, and fold-and-thrust belt propagation was coeval with angular unconformity development and deposition of the coarse-grained conglomeratic to sandy lowermost Umpqua Group (Wells et al., 2000, 2014). The syn-collisional Umpqua Group is over 3 km thick, and this overall greater thickness of syn-collisional strata compared to that of the Lyre Formation is likely related to differing deformation styles due to changes in plateau thickness along strike.

Siletzia was still extremely young (0–6 m.y.) and actively erupting during collision, which resulted in its buoyant and weak rheological behavior (Cloos, 1993; Mason et al., 2010; Vogt and Gerya, 2014; Tao et al., 2020; Liu et al., 2021). In Washington and on southern Vancouver Island, the collision resulted in a short-lived topographic response that led to creation of the Cowichan fold-and-thrust belt and deformation of preexisting forearc basin strata inboard of the suture (England and Calon, 1991; Johnston and Acton, 2003; Eddy et al., 2016). East of the suture, exhumation of the Western Mélange Belt resulted in the development of unconformity and reversal of paleocurrent from east-derived to west-derived sediment in the Upper Swauk Formation (Eddy et al., 2016), similar to the influx of Western Mélange Belt-derived detritus in Lower Lyre Formation sandstone west of the suture. These relationships indicate that the Western Mélange Belt served as a topographic barrier between the two basins and is consistent with low-temperature thermochronologic data suggesting 3–4 km of vertical uplift of the Cowichan fold-and-thrust belt (England and Calon, 1991). However, although this was a significant topographic response, a major long-lived mountain-building event like those seen in collisions of oceanic plateaus in Alaska, USA (Yakutat; Pavlis et al., 2004; Finzel et al., 2011; Elliott et al., 2013), and South America (Caribbean; León et al., 2021) did not

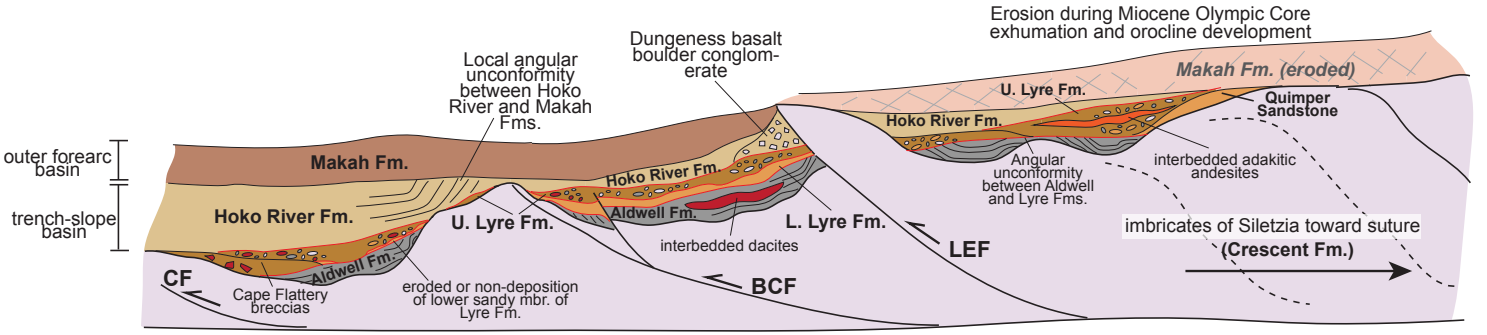

Figure 10. Tectonostratigraphic cross-section of the peripheral rock sequence and basement Crescent basalt showing the distribution of units across the northern Olympic Peninsula. Periods of deformation associated with the Lower Elwha Fault (LEF), Boundary Creek Fault (BCF), and Crescent Fault (CF) were synchronous with deposition of the Lyre and Hoko River formations in the middle to late Eocene. These phases of deformation are associated with construction of the early subduction complex following Siletzia's collision, and an influx of continentally derived sediment led to the integration of basin deposits in a regional forearc basin known as the Tofino–Juan de Fuca basin. Later Miocene deformation associated with orocline development and exhumation of the Olympic subduction complex led to reactivation of the Lower Elwha Fault, Boundary Creek Fault, and Crescent Fault and exhumation and erosion of overlying rocks of the peripheral rock sequence. L.—lower; U.—upper.

occur. In these collisions, oceanic plateaus collided over 30 m.y. after their formation, and flat-slab subduction of the plateau occurred up to hundreds of kilometers inboard of the trench, which resulted in rapid exhumation and long-lived fold-and-thrust belt development. Extensive thermochronologic studies document rapid exhumation of the Wrangell–St. Elias mountains in Alaska since the Oligocene (O'Sullivan et al., 1997; Berger et al., 2008; Enkelmann et al., 2008, 2009, 2010; McAleer et al., 2009; Spotila and Berger, 2010; Falkowski et al., 2014). For example, zircon fission-track analyses from 2 Ma to 3 Ma zircon are estimated to have originated from depths of 5–10 km, mandating rapid exhumation in <5 m.y. (Enkelmann et al., 2009). This indicates that flat-slab subduction of the Yakutat terrane resulted in long-lived (>25–30 m.y.) and regionally extensive deformation (hundreds of kilometers inboard) relative to the shorter collisional period (3–5 m.y.) associated with slab breakoff and outboard migration of the subduction zone observed for Siletzia in this study. These differences may help to explain why extensive preaccretion hemipelagic strata of the Aldwell Formation were preserved during the collisional process (Fig. 10). Therefore, identification of extensive preaccretion deposits could be important in recognizing sedimentary records of young oceanic plateau collision.

In contrast to flat-slab subduction and long-lived deformation associated with older plateaus, slab breakoff and outboard migration of the trench characterized the collision and accretion of the young, buoyant Siletzia plateau (Fig. 8). We interpret accretion of Siletzia and outboard migration of the trench to have occurred by ca. 47 Ma, and to be marked by the development of an unconformity between the lower sandy and upper conglomeratic members of the Lyre Formation (Fig. 10). Development of an unconformity between the lower and upper members of the Lyre Formation is constrained by ca. 47–46.5 Ma dates from interbedded andesites in the upper conglomeratic member (Fig. 10). Imbricated thrust sheets of Siletzia were immediately incorporated into the newly formed subduction complex (Fig. 8). At new convergent margins, subduction initiation can be associated with a period of exhumation (conglomeratic deposition) at the trench followed by rapid subsidence and deep-water sedimentation (Rains et al., 2012). This is similar to the observed transition from the Upper Lyre to Hoko River formations (Fig. 10). Additionally, volcanism is documented to occur much closer to the trench during initiation at a prearc stage (Patriat et al., 2019), and in the case of subduction of oceanic plateaus, intermediate volcanic rocks are thought to commonly mark subduction initiation (Seyler et al., 2021). The presence of 47–46.5 Ma intermediate volcanics and adakites interbedded with the upper conglomeratic member of the Lyre Formation could be the result of newly established subduction beneath the plateau or the presence of the slab edge, tear, or window (Thorkelson and Taylor, 1989; Ickert et al., 2009; Tepper and Clark, 2024; Tepper et al., 2024; Anderson et al., 2024). In summary, following the accretion of young oceanic plateaus, short-lived deformation can be followed by rapid outboard migration of the trench. Sediments on the newly accreted plateau are initially deposited in isolated trench-slope basins derived from primarily local sources before transitioning to a fully integrated forearc basin with a higher proportion of continentally derived detritus (Fig. 10). This transition is accommodated by continued regional thermal subsidence following the accretion and cooling of the young oceanic plateau.

CONCLUSIONS

Our results demonstrate distinct stages of basin development before, during, and after collision of the Siletzia oceanic plateau along the northern Olympic Peninsula. There were four main stages of deformation and basin development.

(1) A precollisional stage is characterized by massive siltstone of the Aldwell Formation deposited in isolated basins on top of basaltic flows of Siletzia.

(2) A syn-collisional stage deformed preaccretion units in a west-verging fold-and-thrust belt, and led to angular unconformity development and deposition of the lower member of the Lyre Formation across the unconformity. Outboard migration of the trench occurred by ca. 47–46.5 Ma, and boulder–pebble conglomerates of the Upper Lyre Formation were interbedded with adakites and deposited on top of imbricated basement basalts in structurally controlled trench-slope basins. The locations of these trench-slope basins were related to preexisting oceanic plateau topography and new topography created by the active fold-thrust belt on the newly formed subduction complex comprising the imbricated slivers of accreted Siletzia basalts following outboard trench migration.

(3) The postcollisional stage was marked by deposition of mass transport and olistostromal units of the Lower Hoko River Formation in isolated trench-slope basins that were deriving sediments primarily from locally exhumed Siletzia basement basalts. Continued faulting and segmentation of basins on the outer portion of the subduction complex during this time are likely related to the subduction of seamounts. Deposition of the middle to Upper Hoko River Formation records the infilling of isolated trench-slope basins that were primarily deriving sediments from local sources, and the beginning stages of an influx of sediments derived from continental sources.

(4) During the fourth stage, continued thermal subsidence of the accreted plateau led to a transition from isolated trench-slope basins to continentally derived forearc basin deposits of the Makah Formation by ca. 35 Ma. These strata are part of the regional Tofino–Juan de Fuca forearc basin and correlate to age-equivalent strata on and adjacent to Vancouver Island. Sediments in this basin were derived primarily from continental sources in British Columbia, Vancouver Island, and western Washington, and represent a natural extension of the upper watershed to access a greater region through time. More broadly, the Siletzia oceanic plateau was still being constructed as it collided with the continental margin, making it rheologically weak and buoyant. Therefore, the sedimentary and structural response recorded in the northern peripheral rock sequence is unique to this style of oceanic plateau collision. Establishing a detailed sedimentary and structural framework for the collision of young and buoyant oceanic plateaus is critical for recognizing these events elsewhere in the geologic record.

ACKNOWLEDGMENTS

We thank Nick Borders, Sam Brockschmidt, Jason Muhlbauer, and Nick Regier for their assistance in the field. Additionally, we thank Adriana Brown, Rachel Culver, and Luke McCreary for their assistance in mineral separation and collecting geochronologic data. We also thank the Arizona LaserChron Center for helping analyze samples for LA-ICP-MS. Specifically, we thank Wai Allen, Daniel Alberts, Michelle Foley, George Gehrels, Mauricio Ibañez-Mejia, Tom Milster, and Mark Pecha. We thank Nick Zentner for highlighting this research in his outreach efforts and for connecting us with local individuals who aided in land access. Financial support for this project was provided by National Science Foundation grant EAR-2151277 to Michael Eddy and Ken Ridgway. This research was further supported by graduate research grants to Erin Donaghy from the National Science Foundation's EarthRates, the Evolving Earth Foundation, the Geological Society of America, the Lewis and Clark Fund for Exploration and Field Research, and Purdue University. We would like to thank Olympic National Park for their support in this research and access to park resources. We also thank Campbell Global, Green Crow, Hampton Lumber, and Merrill and Ring for their support in this research and access to logging roads and land. The manuscript has benefited from the thoughtful comments of reviewers Cathy Busby and Michael Darin, and editorial feedback from Associate Editor Mark E. Holland and Science Editor David E. Fastovsky.

REFERENCES CITED

Anderson, M.L., Blakely, R.J., Wells, R.E., and Dragovich, J.D., 2024, Deep structure of Siletzia in the Puget Lowland: Imaging an obducted plateau and accretionary thrust belt with potential fields: Tectonics, v. 43, https://doi.org/10.1029/2022TC007720.

Ansfield, V.J., 1972, The stratigraphy and sedimentology of the Lyre Formation, northwestern Olympic Peninsula, Washington [M.S. thesis]: Seattle, University of Washington, 130 p.

Babcock, R.S., Burmester, R.R., Engebretson, D.C., Warnock, A.C., and Clark, K.P., 1992, A rifted margin origin for the Crescent basalts and related rocks in the northern Coast Range Volcanic Province, Washington and British Columbia: Journal of Geophysical Research: Solid Earth, v. 97, p. 6799–6821, https://doi.org/10.1029/91JB02926.

Babcock, R.S., Suczek, C.A., and Engebretson, D.C., 1994, The Crescent "Terrane", Olympic Peninsula and Southern Vancouver Island: Washington Division of Geology and Earth Resources Bulletin, v. 80, p. 141–157.

Ballard, R.D., Holcomb, R.T., and Van Andel, T.H., 1979, The Galapagos Rift at 86°W: 3. Sheet flows, collapse pits, and lava lakes of the Rift Valley: Journal of Geophysical Research: Solid Earth, v. 84, p. 5407–5422, https://doi.org/10.1029/JB084iB10p05407.

Beikman, H.H., Rau, W.W., and Wagner, H.C., 1967, The Lincoln Creek Formation, Grays Harbor Basin, Southwestern Washington: U.S. Geological Survey Bulletin 1244-I, 14 p.

Berger, A.L., Spotila, J.A., Chapman, J.B., Pavlis, T.L., Enkelmann, E., Ruppert, N.A., and Buscher, J.T., 2008, Architecture, kinematics and exhumation of a convergent orogenic wedge: A thermochronologic investigation of tectonic-climatic interactions within the central St. Elias orogen, Alaska: Earth and Planetary Science Letters, v. 270, p. 13–24, https://doi.org/10.1016/j.epsl.2008.02.034.

Brandon, M., and Massey, N.W.D., 1985, Early Tertiary tectonics of the Pacific Northwest: Truncation and rifting within a transform plate boundary [abstract]: Geological Association of Canada Program and Abstracts, p. 8–9.

Brandon, M.T., and Calderwood, A.R., 1990, High-pressure metamorphism and uplift of the Olympic subduction complex: Geology, v. 18, p. 1252–1255, https://doi.org/10.1130/0091-7613(1990)018<1252:HPMAUO>2.3.CO;2.

Brandon, M.T., and Vance, J.A., 1992a, Tectonic evolution of the Cenozoic Olympic Subduction Complex, Washington State, as deduced from fission track ages for detrital zircons: American Journal of Science, v. 292, p. 565–636, https://doi.org/10.2475/ajs.292.8.565.

Brandon, M.T., and Vance, J.A., 1992b, Zircon fission-track ages for the Olympic subduction complex and adjacent Eocene basins, western Washington State: Washington State Division of Geology and Earth Resources Open File Report 92–6.

Brown, R.D., Jr., and Gower, H.D., 1958, Twin River Formation (redefinition), northern Olympic Peninsula, Washington: The American Association of Petroleum Geologists Bulletin, v. 42, p. 2492–2512.

Brown, R.D., and Gower, R.D., 1960, Geology of the Port Angeles-Lake Crescent area, Clallam County, Washington: U.S. Geological Survey Oil and Gas Investigation Series Map OM- 203, scale 1:62,500, https://doi.org/10.3133/om203.

Brown, R.D., Jr., Snavely, P.D., Jr., and Gower, H.D., 1956, Lyre Formation (Redefinition), northern Olympic Peninsula, Washington: American Association of Petroleum Geologists Bulletin, v. 40, p. 94–107.

Cady, W.M., 1975, Tectonic setting of Tertiary volcanic rocks of the Olympic Peninsula, Washington: Journal of Research of the U.S. Geological Survey, v. 3, p. 573–582.

Cady, W.M., Tabor, R.W., MacLeod, N.S., and Sorenson, M.L., 1972, Geologic map of the Tyler Peak quadrangle, Clallam and Jefferson Counties, Washington: U.S. Geological Survey Geologic Quadrangle 970, scale 1:62,500, 1 plate, https://doi.org/10.3133/gq970.

Cecil, M.R., Rusmore, M.E., Gehrels, G.E., Woodsworth, G.J., Stowell, H.H., Yokelson, I.N., Chisom, C., Trautman, M., and Homan, E., 2018, Along-strike variation in the magmatic tempo of the Coast Mountain Batholith, British Columbia, and implications for processes controlling episodicity in arcs: Geochemistry, Geophysics, Geosystems, v. 19, p. 4274–4289, https://doi.org/10.1029/2018GC007874.

Ciborowski, T.J.R., Phillips, B.A., Kerr, A.C., Barfod, D.N., and Mark, D.F., 2020, Petrogenesis of Siletzia: The world's youngest oceanic plateau: Results in Geochemistry, v. 1, https://doi.org/10.1016/j.ringeo.2020.100004.

Clark, K.P., 1989, The stratigraphy and geochemistry of the Crescent Formation basalts and the bedrock geology of associated igneous rocks near Bremerton Washington [M.S. thesis]: Bellingham, Western Washington University, 171 p.

Cloos, M., 1993, Lithospheric buoyance and collisional orogenesis: Subduction of oceanic plateaus, continental margins, island arcs, spreading ridges, and seamounts: Geological Society of America Bulletin, v. 105, p. 715–737, https://doi.org/10.1130/0016-7606(1993)105<0715:LBACOS>2.3.CO;2.

Clowes, R.M., Brandon, M.T., Green, A.G., Yorath, C.J., Sutherland, A., Kanasewich, E.R., and Spencer, C., 1987, LITHOPROBE—Southern Vancouver Island: Cenozoic subduction complex imaged by deep seismic reflections: Canadian Journal of Earth Sciences, v. 24, p. 31–51, https://doi.org/10.1139/e87-004.

Condon, D.J., McLean, N., Schoene, B., Bowring, S., Parrish, R.R., and Noble, S., 2008, Synthetic U-Pb "standard" solutions for ID-TIMS geochronology: Geochimica et Cosmochimica Acta, v. 72, p. A175.

Coutts, D.S., Matthews, W.A., Englert, R.G., Brooks, M.D., Boivin, M.P., and Hubbard, S.M., 2020, Along-strike variations in sediment provenance within the Nanaimo basin reveal mechanisms of forearc basin sediment influx events: Lithosphere, v. 12, p. 180–197, https://doi.org/10.1130/L1138.1.

Darin, M.H., Armentrout, J.M., and Dorsey, R.J., 2022, Oligocene onset of uplift and inversion of the Cascadia forearc basin, southern Oregon Coast Range, USA: Geology, v. 50, p. 603–609, https://doi.org/10.1130/G49925.1.

Davy, B., Hoernle, K., and Werner, R., 2008, Hikurangi Plateau: Crustal structure, rifted formation, and Gondwana subduction history: Geochemistry, Geophysics, Geosystems, v. 9, https://doi.org/10.1029/2007GC001855.

DeChant, J.H., 1989, Sedimentary petrology, depositional environment, and paleogeographic significance of the upper Eocene Hoko River Formation, northern Olympic Peninsula, Washington [M.S. thesis]: Bellingham, Western Washington University, 195 p.

Donaghy, E.E., Eddy, M.P., Moreno, F., and Ibañez-Mejia, M., 2024, Minimizing the effects of Pb loss in detrital and igneous U-Pb geochronology by CA-LA-ICP-MS: Geochronology, v. 6, p. 89–106, https://doi.org/10.5194/gchron-6-89-2024.

Dragovich, J.D., Littke, H.A., Anderson, M.L., Hartog, R., Wessel, G.R., DuFrane, S.A., Walsh, T.J., MacDonald, J.H., Jr., Mangano, J.F., and Cakir, R., 2009, Geologic map of the Snoqualmie 7.5-minute quadrangle, King County, Washington: Washington Division of Geology and Earth Resources Geology Map GM-75, scale 1:24,000, 2 sheets.

Duncan, R.A., 1982, A captured island chain in the coast range of Oregon and Washington: Journal of Geophysical Research: Solid Earth, v. 87, p. 10,827–10,837, https://doi.org/10.1029/JB087iB13p10827.

Durham, J.W., 1944, Megafaunal zones of the Oligocene of northwestern Washington: University of California Publications, Bulletin of the Department of Geological Sciences, v. 27, no. 5, p. 101–212.

Eddy, M.P., Bowring, S.A., Umhoefer, P.J., Miller, R.B., McLean, N.M., and Donaghy, E.E., 2016, High-resolution temporal and stratigraphic record of Siletzia's accretion and triple junction migration from nonmarine sedimentary basins in central and western Washington: Geological Society of America Bulletin, v. 128, p. 425–441, https://doi.org/10.1130/B31335.1.

Eddy, M.P., Clark, K.P., and Polenz, M., 2017, Age and volcanic stratigraphy of the Eocene Siletzia oceanic plateau in Washington and on Vancouver Island: Lithosphere, v. 9, p. 652–664, https://doi.org/10.1130/L650.1.

Einarsen, J.M., 1987, The petrography and tectonic significance of the Blue Mountain unit, Olympic Peninsula, Washington [M.S. thesis]: Bellingham, Western Washington University, 175 p.
Elliott, J., Freymueller, J.T., and Larsen, C.F., 2013, Active tectonics of the St. Elias orogen, Alaska, observed with GPS measurements: Journal of Geophysical Research: Solid Earth, v. 118, p. 5625–5642, https://doi.org/10.1002/jgrb.50341.
England, T.D.J., and Calon, T.J., 1991, The Cowichan fold and thrust system, Vancouver Island, southwestern British Columbia: Geological Society of America Bulletin, v. 103, p. 336–362, https://doi.org/10.1130/0016-7606(1991)103<0336:TCFATS>2.3.CO;2.
Enkelmann, E., Garver, J.I., and Pavlis, T.L., 2008, Rapid exhumation of ice-covered rocks of the Chugach-St. Elias orogen, SE-Alaska: Geology, v. 36, p. 915–918, https://doi.org/10.1130/G2252A.1.
Enkelmann, E., Zeitler, P.K., Pavlis, T.K., Garver, J.I., and Ridgway, K.D., 2009, Intense localized rock uplift and erosion in the St Elias orogen of Alaska: Nature Geoscience, v. 2, p. 360–363, https://doi.org/10.1038/ngeo502.
Enkelmann, E., Zeitler, P.K., Garver, J.I., Pavlis, T.L., and Hooks, B.P., 2010, The thermochronological record of tectonic and surface process interaction at the Yakutat-North American collision zone in Southeast Alaska: American Journal of Science, v. 310, p. 231–260, https://doi.org/10.2475/04.2010.01.
Fairchild, L.H., and Cowan, D.S., 1982, Structure, petrology, and tectonic history of the Leech River Complex northwest of Victoria, Vancouver Island: Canadian Journal of Earth Sciences, v. 19, no. 9, https://doi.org/10.1139/e82-161.
Falkowski, S., Enkelmann, E., and Ehlers, T.A., 2014, Constraining the area of rapid and deep-seated exhumation at the St. Elias syntaxis, Southeast Alaska, with detrital zircon fission-track analysis: Tectonics, v. 33, p. 597–616, https://doi.org/10.1002/2013TC003408.
Faugères, J.C., Legigan, P., Maillet, N., and Latouche, C., 1989, Pelagic, turbiditic, and contouritic sequential deposits on the Cape Verde Plateau (Leg 108, Site 659, Northwest Africa): Sediment record during Neogene Time, *in* Ruddiman, W., and Sarnthein, M., eds., Proceedings of the Ocean Drilling Program: College Station, Texas, Ocean Drilling Program Scientific Results, v. 108.
Festa, A., Barbero, E., Remitti, F., Ogata, K., and Pini, G.A., 2022, Mélanges and chaotic rock units: Implications for exhumed subduction complexes and orogenic belts: Geosystems and Geoenvironment, v. 1, https://doi.org/10.1016/j.geogeo.2022.100030.
Finzel, E.S., Trop, J.M., Ridgway, K.D., and Enkelmann, E., 2011, Upper plate proxies for flat-slab subduction processes in southern Alaska: Earth and Planetary Science Letters, v. 303, p. 348–360, https://doi.org/10.1016/j.epsl.2011.01.014.
Frey, F.A., Coffin, M.F., Wallace, P.J., Weis, D., Zhao, X., Wise, S.W., Jr., Wahnert, V., Teagle, D.A.H., Saccocia, P.J., Reusch, D.N., Pringle, M.S., Nicolaysen, K.E., Neal, C.R., Muller, R.D., Moore, C.L., Mahoney, J.J., Keszthelyi, L., Inokuchi, H., Duncan, R.A., Delius, H., Damuth, J.E., Damasceno, D., Coxall, H.K., Borre, M.K., Boehm, F., Barling, J., Arndt, N.T., and Antretter, M., 2000, Origin and evolution of a submarine large igneous province: The Kerguelen Plateau and Broken Ridge, southern Indian Ocean: Earth and Planetary Science Letters, v. 176, p. 73–89, https://doi.org/10.1016/S0012-821X(99)00315-5.
Gao, H., Humphreys, E.D., Yao, H., and van der Hilts, R.D., 2011, Crust and lithosphere structure of the northwestern U.S. with ambient noise tomography: Terrane accretion and Cascade arc development: Earth and Planetary Science Letters, v. 304, p. 202–211, https://doi.org/10.1016/j.epsl.2011.01.033.
Garver, J.I., and Brandon, M.T., 1994, Erosional denudation of the British Columbia Coast Ranges as determined from fission-track ages of detrital zircon from the Tofino basin, Olympic Peninsula, Washington: Geological Society of America Bulletin, v. 106, p. 1398–1412, https://doi.org/10.1130/0016-7606(1994)106<1398:EDOTBC>2.3.CO;2.
Gladczenko, T.P., and Coffin, M.F., 2001, Kerguelen Plateau crustal structure and basin formation from seismic and gravity data: Journal of Geophysical Research: Solid Earth, v. 106, p. 16,583–16,601, https://doi.org/10.1029/2001JB000370.
Greene, A.R., Scoates, J.S., Weis, D., Katvala, E.C., Israel, S., and Nixon, G.T., 2010, The architecture of oceanic plateaus revealed by the volcanic stratigraphy of the accreted Wrangellia oceanic plateau: Geosphere, v. 6, p. 47–73, https://doi.org/10.1130/GES00212.1.
Gregg, T.K.P., and Fink, J.H., 1995, Quantification of submarine lava-flow morphology through analog experiments: Geology, v. 23, p. 73–76, https://doi.org/10.1130/0091-7613(1995)023<0073:QOSLFM>2.3.CO;2.
Groome, W.G., Thorkelson, D.J., Friedman, R.M., Mortensen, J.K., Massey, N.W.D., Marschall, D.D., and Layer, P.W., 2003, Magmatic and tectonic history of the Leech River Complex, Vancouver Island, British Columbia: Evidence for ridge-trench intersection and accretion of the Crescent terrane, *in* Sisson, V.B., et al., eds., Geology of a Transpressional Orogen Developed during Ridge-Trench Interaction along the North Pacific Margin: Geological Society of America Special Paper 371, p. 327–353, https://doi.org/10.1130/0-8137-2371-X.327.
Hyndman, R.D., Yorath, C.J., Clowes, R.M., and Davis, E.E., 1990, The northern Cascadia subduction zone at Vancouver Island: Seismic structure and tectonic history: Canadian Journal of Earth Sciences, v. 27, p. 313–329, https://doi.org/10.1139/e90-030.
Ickert, R.B., Thorkelson, D.J., Marshall, D.D., and Ullrich, T.D., 2009, Eocene adakitic volcanism in southern British Columbia: Remelting of arc basalt above a slab window: Tectonophysics, v. 464, p. 164–185, https://doi.org/10.1016/j.tecto.2007.10.007.
Irving, E., and Brandon, M.T., 1990, Paleomagnetism of the Flores volcanics: Vancouver Island in place by Eocene time: Canadian Journal of Earth Sciences, v. 27, p. 811–817, https://doi.org/10.1139/e90-083.
Jett, G.A., and Heller, P.L., 1988, Tectonic significance of polymodal compositions in mélange sandstones, Western Mélange Belt, North Cascades Range, Washington: Journal of Sedimentary Petrology, v. 58, p. 52–61.
Johnston, S.T., and Acton, S., 2003, The Eocene southern Vancouver Island orocline—A response to seamount accretion and the cause of fold-and-thrust belt and extensional basin formation: Tectonophysics, v. 365, p. 165–183, https://doi.org/10.1016/S0040-1951(03)00021-0.
Johnson, S.Y., 1985, Eocene strike-slip faulting and nonmarine basin formation in Washington, *in* Biddle, K.T., and Christie-Blick, N., eds., Strike-Slip Deformation, Basin Formation and Sedimentation: Society of Economic Paleontologists and Mineralogists Special Publication 37, p. 283–302, https://doi.org/10.2110/pec.85.37.0283.
Jovane, L., Figueiredo, J.J., Alves, D.P.V., Lacopini, D., Giorgioni, M., Vannucchi, P., Moura, D.S., Bezerra, F.H.R., Vital, H., Rios, I.L.A., and Molina, E.C., 2016, Seismostratigraphy of the Ceará Plateau: Clues to decipher the Cenozoic evolution of Brazilian equatorial margin: Frontiers of Earth Science, v. 4, https://doi.org/10.3389/feart.2016.00090.
Kant, L.B., Tepper, J.H., and Nelson, B.K., 2018, Eocene basalt of Summit Creek: Slab breakoff magmatism in the central Washington Cascades, USA: Lithosphere, v. 10, p. 792–805, https://doi.org/10.1130/L731.1.
Kerr, A.C., 2014, Oceanic plateaus, *in* Holland, H.C., Turekian, K., and Rudnick, R., eds., Treatise on Geochemistry, Volume 4: The Crust (2nd edition): Elsevier, p. 631–667.
Kerr, A.C., and Mahoney, J.J., 2007, Oceanic plateaus: Problematic plumes, potential paradigms: Chemical Geology, v. 241, p. 332–353, https://doi.org/10.1016/j.chemgeo.2007.01.019.
Kerr, A.C., and Tarney, J., 2005, Tectonic evolution of the Caribbean and northwestern South America: The case for accretion of two Late Cretaceous oceanic plateaus: Geology, v. 33, p. 269–272, https://doi.org/10.1130/G21109.1.
Kerr, A.C., Marriner, G.F., Arndt, N.T., Tarney, J., Nivia, A., Saunders, A.D., and Duncan, R.A., 1996, The petrogenesis of Gorgona komatiites, picrites and basalts: New field, petrographic and geochemical constraints: Lithosphere, v. 37, p. 245–260.
Kerr, A.C., White, R.V., Thompson, P.M.E., Tarney, J., and Saunders, A.D., 2003, No oceanic plateau—No Caribbean Plate? The seminal oceanic plateau in Caribbean Plate evolution, *in* Bartolini, C., Buffler, R.T., and Blickwede, J.F., eds., The Circum-Gulf of Mexico and the Caribbean: Hydrocarbon Habitats, Basin Formation, and Plate Tectonics: AAPG Memoir 79, https://doi.org/10.1306/M79877C6.
Laursen, J., Scholl, D.W., and von Huene, R., 2002, Neotectonic deformation of the central Chile deepwater forearc basin formation in response to hot spot ridge and seamount subduction: Tectonics, v. 21, p. 2-1–2-27, https://doi.org/10.1029/2001TC901023.
León, S., Monsalve, G., and Bustamante, C., 2021, How much did the Colombian Andes rise by the collision of the Caribbean oceanic plateau?: Geophysical Research Letters, v. 48, https://doi.org/10.1029/2021GL093362.
Liu, L., Gurnis, M., Seton, M., Saleeby, J., Müller, R.D., and Jackson, J.M., 2010, The role of oceanic plateau subduction in the Laramide orogeny: Nature Geoscience, v. 3, p. 353–357, https://doi.org/10.1038/ngeo829.
Liu, Z., Dai, L., Li, S., Wang, L., Xing, H., Liu, Y., Ma, F., Dong, H., and Li, F., 2021, When plateau meets subduction zone: A review of numerical models: Earth-Science Reviews, v. 215, https://doi.org/10.1016/j.earscirev.2021.103556.
MacLeod, N.S., Tiffin, D.L., Snavely, P.D., Jr., and Currie, R.G., 1977, Geologic interpretation of magnetic and gravity anomalies in the Strait of Juan de Fuca: Canadian Journal of Earth Sciences, v. 14, p. 223–238, https://doi.org/10.1139/e77-024.
Madsen, J.K., Thorkelson, D.J., Friedman, R.M., and Marshall, D.D., 2006, Cenozoic to Recent plate configurations in the Pacific basin: Ridge subduction and slab window magmatism in western North America: Geosphere, v. 2, p. 11–34, https://doi.org/10.1130/GES00020.1.

Mallory, V.S., 1959, Lower Tertiary Biostratigraphy of the California Coast Ranges: Tulsa, Oklahoma, American Association of Petroleum Geologists Special Publication, 416 p., https://doi.org/10.1306/SV20351.
Mann, P., and Taira, A., 2004, Global tectonic significance of the Solomon Islands and Ontong Java Plateau convergent zone: Tectonophysics, v. 389, p. 137–190, https://doi.org/10.1016/j.tecto.2003.10.024.
Marcott, K., 1984, The sedimentary petrography, depositional environment and tectonic setting of the Aldwell Formation, Northern Olympic Peninsula, Washington [M.S. thesis]: Bellingham, Western Washington University, 78 p.
Mason, W.G., Moresi, L., Betts, P.G., and Miller, M.S., 2010, Three-dimensional numerical models of the influence of a buoyant oceanic plateau on subduction zones: Tectonophysics, v. 483, p. 71–79, https://doi.org/10.1016/j.tecto.2009.08.021.
Massari, F., and Colella, A., 1988, Evolution and types of fan-delta systems in some major tectonic setting, *in* Nemec, W., and Steel, R.J., eds., Fan Deltas: Sedimentology and Tectonic Setting: Blackie & Son, p. 103–122.
Massey, N.W.D., 1986, Metchosin igneous complex, southern Vancouver Island: Ophiolite stratigraphy developed in an emergent island setting: Geology, v. 14, p. 602–605, https://doi.org/10.1130/0091-7613(1986)14<602:MICSVI>2.0.CO;2.
Matthews, W.A., Guest, B., Coutts, D., Bain, H., and Hubbard, S., 2017, Detrital zircons from the Nanaimo basin, Vancouver Island, British Columbia: An independent test of Late Cretaceous to Cenozoic northward translation: Tectonics, v. 36, p. 854–876, https://doi.org/10.1002/2017TC004531.
Mattinson, J.M., 2005, Zircon U–Pb chemical-abrasion ("CA-TIMS") method: Combined annealing and multi-step dissolution analysis for improved precision and accuracy of zircon ages: Chemical Geology, v. 220, p. 47–66, https://doi.org/10.1016/j.chemgeo.2005.03.011.
McAleer, R.J., Spotila, J.A., Enkelmann, E., and Berger, A.L., 2009, Exhumation along the Fairweather Fault, southeastern Alaska, based on low-temperature thermochronometry: Tectonics, v. 28, https://doi.org/10.1029/2007TC002240.
McKanna, A.J., Koran, I., Schoene, B., and Ketcham, R.A., 2023, Chemical abrasion: The mechanics of zircon dissolution: Geochronology, v. 5, p. 127–151, https://doi.org/10.5194/gchron-5-127-2023.
McWilliams, R.G., 1970, Evidence for thrust faulting in northern Olympic Peninsula, Washington: The American Association of Petroleum Geologists Bulletin, v. 54, p. 344–349.
Miller, R.B., Gordon, S.M., Bowring, S.A., Doran, B.A., McLean, N., Michels, Z., Shea, E., and Whitney, D.L., 2016, Linking deep and shallow crustal processes during regional transtension in an exhumed continental arc, North Cascades, northwestern Cordillera (USA): Geosphere, v. 12, p. 900–924, https://doi.org/10.1130/GES01262.1.
Miller, R.B., Umhoefer, P.J., Eddy, M.P., and Tepper, J.H., 2023, Upper-plate response to ridge subduction and oceanic plateau accretion, Washington Cascades and surrounding region: Implications for plate tectonic evolution of the Pacific Northwest (USA and southwestern Canada) in the Paleogene: Geosphere, v. 19, p. 1157–1179, https://doi.org/10.1130/GES02629.1.
Munschy, M., Rotstein, Y., Schlich, R., and Coffin, M.F., 1993, Structure and tectonic setting of the 77°E and 75°E grabens, Kerguelen Plateau, South Indian Ocean: Journal of Geophysical Research: Solid Earth, v. 98, p. 6367–6382, https://doi.org/10.1029/92JB02694.
Nemchin, A., and Cawood, P., 2005, Discordance of the U-Pb system in detrital zircons: Implication for provenance studies of sedimentary rocks: Sedimentary Geology, v. 182, p. 143–162, https://doi.org/10.1016/j.sedgeo.2005.07.011.
Oliveira, A.L., Schmitz, M.D., Wall, C.J., Crowley, J.L., Macêdo Filho, A.A., and Hollanda, M.H.B.M., 2023, New U-Pb geochronology for the Central Atlantic Magmatic Province, critical reevaluation of high-precision ages and their impact on the end-Triassic extinction event: Scientific Reports, v. 13, https://doi.org/10.1038/s41598-023-32534-3.
O'Sullivan, P.B., Plafker, G., and Murphy, J.M., 1997, Apatite fission-track thermotectonic history of crystalline rocks in the northern Saint Elias Mountains, Alaska, *in* Dumoulin, J.A., and Gray, J.E., eds., Geological studies in Alaska by the U.S. Geological Survey: U.S. Geological Survey Professional Paper 154, p. 283–294.
Patriat, M., Falloon, T., Danyushevsky, L., Collot, J., Jean, M.M., Hoernle, K., Hauff, F., Maas, R., Woodhead, J.D., and Feig, S.T., 2019, Subduction initiation terranes exposed at the front of a 2 Ma volcanically-active subduction zone: Earth and Planetary Science Letters, v. 508, p. 30–40, https://doi.org/10.1016/j.epsl.2018.12.011.
Pavlis, T.L., Picornell, C., Serpa, L., Bruhn, R.L., and Plafker, G., 2004, Tectonic processes during oblique collision: Insights from the St. Elias orogen, northern North America Cordillera: Tectonics, v. 23, https://doi.org/10.1029/2003TC001557.
Parrish, R.R., 1983, Cenozoic thermal evolution and tectonics of the Coast Mountains of British Columbia. 1. Fission track dating, apparent uplift rates, and patterns of uplift: Tectonics, v. 2, p. 601–631, https://doi.org/10.1029/TC002i006p00601.
Petterson, M.G., Neal, C.R., Mahoney, J.J., Kroenke, L.W., Saunders, A.D., Babbs, T.L., Duncan, R.A., Tolia, D., and McGrail, B., 1997, Structure and deformation of north and central Malaita, Solomon Islands: Tectonic implications for the Ontong Java Plateau-Solomon arc collision, and for the fate of oceanic plateaus: Tectonophysics, v. 283, p. 1–33, https://doi.org/10.1016/S0040-1951(97)00206-0.
Phillips, B.A., Kerr, A.C., Mullen, E.K., and Weis, D., 2017, Oceanic mafic magmatism in the Siletz terrane, NW North America: Fragments of an Eocene oceanic plateau?: Lithosphere, v. 274–275, p. 291–303, https://doi.org/10.1016/j.lithos.2017.01.005.
Polenz, M., Wegmann, K.W., and Schasse, H.W., 2004, Geologic map of the Elwha and Angeles Point 7.5-minute quadrangles, Clallam County, Washington: Washington Division of Geology and Earth Resources Open File Report 2004–14, 1:24,000 scale.
Pullen, A., Ibañez-Mejia, M., Gehrels, G.E., Giesler, D., and Pecha, M., 2018, Optimization of a laser ablation-single collector-inductively coupled plasma-mass spectrometer (Thermo Element 2) for accurate, precise, and efficient zircon U-Th-Pb geochronology: Geochemistry, Geophysics, Geosystems, v. 19, p. 3689–3705, https://doi.org/10.1029/2018GC007889.
Rains, J.L., Marsaglia, K.M., and Dunne, G.C., 2012, Stratigraphic record of subduction initiation in the Permian metasedimentary succession of the El Paso Mountains, California: Lithosphere, v. 4, p. 533–552, https://doi.org/10.1130/L165.1.
Rau, W.W., 1964, Foraminifera from the northern Olympic Peninsula, Washington: U.S. Geological Survey Professional Paper 374-G, p. 1–33, 7 plates.
Rau, W.W., 1966, Stratigraphy and foraminifera of the Satsop River area, southern Olympic Peninsula, Washington: Division of Mines and Geology Bulletin 53.
Sauer, K.B., Gordon, S.M., Miller, R.B., Vervoort, J.D., and Fisher, C.M., 2017, Evolution of the Jura-Cretaceous North American Cordilleran margin: Insights from detrital-zircon U-Pb and Hf isotopes of sedimentary units of the North Cascades Range, Washington: Geosphere, v. 13, p. 2094–2118, https://doi.org/10.1130/GES01501.1.
Sauer, K.B., Gordon, S.M., Miller, R.B., Vervoort, J.D., and Fisher, C.M., 2018, Provenance and metamorphism of the Swakane Gneiss: Implications for incorporation of sediment into the deep levels of the North Cascades continental magmatic arc, Washington: Lithosphere, v. 10, p. 460–477, https://doi.org/10.1130/L712.1.
Schaltegger, U., Ovtcharova, M., Gaynor, S.P., Schoene, B., Wotzlaw, J., Davies, J.F.H.L., Farina, F., Greber, N.D., Szymanowski, D., and Chelle-Michou, C., 2021, Long-term repeatability and interlaboratory reproducibility of high-precision ID-TIMS U-Pb geochronology: Science, v. 36, p. 1466–1477.
Schasse, H.W., 2003, Geologic map of the Washington portion of the Port Angeles 1:100,000 quadrangle: Washington Division of Geology and Earth Resources Open File Report 2003–6, scale 1:100,000.
Schmandt, B., and Humphreys, E., 2011, Seismically imaged relict slab from the 55 Ma Siletzia accretion to the northwest United States: Geology, v. 39, p. 175–178, https://doi.org/10.1130/G31558.1.
Schoene, B., Eddy, M.P., Samperton, K.M., Keller, B.C., Keller, G., Adatte, T., and Khadri, S.F.R., 2019, U-Pb constraints on pulsed eruption of the Deccan Traps across the end-Cretaceous mass extinction: Science, v. 363, p. 862–866, https://doi.org/10.1126/science.aau2422.
Seyler, M., Witt, C., Omana, B., Durand, C., Chiaradia, M., Villagomez, D., and Poujol, M., 2021, Late Cretaceous felsic intrusions in oceanic plateau basalts in SW Ecuador: Markers of subduction initiation?: Journal of South American Earth Sciences, v. 110, https://doi.org/10.1016/j.jsames.2021.103348.
Shekut, S., and Licht, A., 2020, Late middle Miocene emergence of the Olympic Peninsula shown by sedimentary provenance: Lithosphere, https://doi.org/10.2113/2020/7040598.
Shilhanek, A.B., 1992, The sedimentology, petrology, and tectonic significance of the middle Eocene Flattery Breccia, Lyre Formation, northwestern Olympic Peninsula, Washington [M.S. thesis]: Bellingham, Western Washington university, 138 p.
Snavely, P.D., Jr., 1983, Peripheral rocks—Tertiary geology of the northwestern part of the Olympic Peninsula, Washington, *in* Muller, J.E., Snavely, P.D., Jr., and Tabor, R.W., The Tertiary Olympic Terrane, Southwest Vancouver Island and Northwest Washington: Geological Association of Canada Field Trip Guidebook 12, p. 6–31.
Snavely, P.D., 1987, Tertiary geologic framework, neotectonics, and petroleum potential of the Oregon-Washington continental margin, *in* Geology and Resource Potential of the Western North America and Adjacent Ocean Basins—Beaufort Sea to Baja California: Circum Pacific Council for Energy and Mineral Resources Earth Science Series, v. 6, p. 305–335.

Snavely, P.D., Jr., and Landu, D.L., 1983, Northwest Olympic Column, *in* Armentrout, J.M., Hull, D.A., Beaulieu, J.V., and Rau, W.W., eds., Correlation of Cenozoic Stratigraphy Units of Western Oregon and Washington: Oregon Department of Geology and Mineral Industries Oil and Gas Investigations 7, p. 66–70.

Snavely, P.D., Jr., MacLeod, N.S., and Wagner, H.C., 1968, Tholeiitic and alkalic basalts of the Eocene Siletz River Volcanics, Oregon Coast Range: American Journal of Science, v. 266, p. 454–481, https://doi.org/10.2475/ajs.266.6.454.

Snavely, P.D., Jr., Pearl, J.E., and Lander, D.L., 1977, Interim report on petroleum resources potential and geologic hazards in the outer continental shelf—Oregon and Washington Tertiary Province: U.S. Geological Survey Open-File Report 77–282, 64 p., https://doi.org/10.3133/ofr77282.

Snavely, P.D., Jr., Niem, A.R., and Pearl, J.E., 1978, Twin River Group (upper Eocene to lower Miocene)—Defined to include the Hoko River, Makah, and Pysht Formations, Clallam County, Washington, *in* Sohl, N.F., and Wright, W.B., Changes in Stratigraphic Nomenclature by the U.S. Geological Survey, 1977: Contributions to Stratigraphy: U.S. Geological Survey Bulletin 1457-A, p. A111–A120.

Snavely, P.D., Jr., Niem, A.R., Macleod, N.S., Pearl, J.W., and Rau, W.W., 1980, Makah Formation—A deep-marginal-basin sequence of late Eocene to Oligocene age in northwestern Olympic Peninsula, Washington: Geological Survey Professional Paper 1162.

Snavely, P.D., Jr., MacLeod, N.S., Niem, A.R., and Minasian, D.L., 1986, Geologic map of Cape Flattery area, Northwestern Olympic Peninsula, Washington: U.S. Geological Survey Open-File Report 86–344B, scale 1:48,000.

Spence, G., Hyndman, R., Langton, S., Davis, E.E., and Yorath, C., 1991, Marine multichannel reflection survey across the northern Cascadia accretionary prism: Geological Survey of Canada Open File Report 2391.

Spotila, J.A., and Berger, A., 2010, Exhumation at orogenic indentor corners under long-term glacial conditions: Example of the St. Elias orogen, Southern Alaska: Tectonophysics, v. 490, p. 241–256, https://doi.org/10.1016/j.tecto.2010.05.015.

Stewart, R.J., and Brandon, M.T., 2004, Detrital-zircon fission-track ages for the "Hoh Formation": Implications for late Cenozoic evolution of the Cascadia subduction wedge: Geological Society of America Bulletin, v. 116, no. 1, p. 60–75, https://doi.org/10.1130/B22101.1.

Tabor, R.W., and Cady, W.M., 1978a, Geological map of the Olympic Peninsula, Washington: U.S. Geological Survey IMAP 994, scale 1:125,000.

Tabor, R.W., and Cady, W.M., 1978b, The structure of the Olympic Mountains, Washington: U.S. Geological Survey IMAP 994, scale 1:125,000.

Tabor, R.W., Frizzell, V.A., Jr., Vance, J.A., and Naeser, C.W., 1984, Ages and stratigraphy of lower and middle Tertiary sedimentary and volcanic rocks of the central Cascades, Washington: Application to the tectonic history of the Straight Creek Fault: Geological Society of America Bulletin, v. 95, p. 26–44, https://doi.org/10.1130/0016-7606(1984)95<26:AASOLA>2.0.CO;2.

Tabor, R.W., Haugerud, R.A., Brown, E.H., Babcock, S.R., and Miller, R.B., 1989, Accreted terranes of the North Cascades Range Washington: International Geologic Congress, 28th, Field Trip Guidebook T3071: Washington, D.C., American Geophysical Union, p. 1–17.

Tao, J., Dai, L., Lou, D., Li, Z.H., Zhou, S., Liu, Z., Li, S., Dong, H., Lan, H., Wang, L., and Li, F., 2020, Accretion of oceanic plateaus at continental margins: Numerical modeling: Gondwana Research, v. 81, p. 390–402, https://doi.org/10.1016/j.gr.2019.11.015.

Taylor, B., 2006, The single largest oceanic plateau: Ontong Java-Manihiki-Hikurangi: Earth and Planetary Science Letters, v. 241, p. 372–380, https://doi.org/10.1016/j.epsl.2005.11.049.

Tepper, J.H., and Clark, K.P., 2024, Initiation of the Cascade arc: Geology, v. 52, p. 297–301, https://doi.org/10.1130/G51888.1.

Tepper, J.H., Clark, K.P., Asmerom, Y., and McIntosh, W.C., 2004, Eocene adakites in the Cascadia forearc: Implications for the position of the Kula-Farallon ridge: Geological Society of America Abstracts with Programs, v. 36, no. 4, p. 69.

Tepper, J.H., Loewen, M.W., Caulfied, L.M., Davidson, P.C., Ruthenberg, K.L., Blakely, S.W.F., Knudsen, D.F.J.F., Black, D.F., Nelson, B.K., and Asmerom, Y., 2024, Petrology and geochronology of Cretaceous–Eocene plutonic rocks in northeastern Washington, USA: Crustal thickening, slab rollback, and origin of the Challis episode: Geological Society of America Bulletin, v. 136, p. 725–740, https://doi.org/10.1130/B36791.1.

Thorkelson, D.J., and Taylor, R.P., 1989, Cordilleran slab windows: Geology, v. 17, p. 833–836, https://doi.org/10.1130/0091-7613(1989)017<0833:CSW>2.3.CO;2.

Trehu, A.M., Asudeh, I., Brocher, T.M., Luetgert, J.H., Mooney, W.D., Nabelek, J.L., and Nakamura, Y., 1994, Crustal architecture of the Cascadia forearc: Science, v. 266, p. 237–243, https://doi.org/10.1126/science.266.5183.237.

Vermeesch, P., 2021, Maximum depositional age estimation revisited: Geoscience Frontiers, v. 12, p. 843–850, https://doi.org/10.1016/j.gsf.2020.08.008.

Vogt, K., and Gerya, T., 2014, From oceanic plateaus to allochthonous terranes: Numerical modelling: Gondwana Research, v. 25, p. 494–508, https://doi.org/10.1016/j.gr.2012.11.002.

Wanless, R.K., Stevens, R.D., Lachance, G.R., and Delabio, R.N., 1978, Age determinations and geological studies, K-Ar isotopic ages: Geological Survey of Canada Report 13, Paper 77-2, 60 p., https://doi.org/10.4095/103387.

Wanless, V.D., Perfit, M.R., Ridley, W.I., and Klein, E., 2010, Dacite petrogenesis on mid-ocean ridges: Evidence for oceanic crustal melting and assimilation: Journal of Petrology, v. 51, https://doi.org/10.1093/petrology/egq056.

Weaver, C.E., 1912, A preliminary report on the Tertiary paleontology of Western Washington: Washington Geological Survey Bulletin 15, 80 p.

Weaver, C.E., 1937, Tertiary stratigraphy of western Washington and northeastern Oregon: Seattle, Washington University Publications in Geology, v. 4, 266 p.

Wells, R., Bukry, D., Friedman, R., Pyle, D., Duncan, R., Haeussler, P., and Wooden, J., 2014, Geologic history of Siletzia, a large igneous province in the Oregon and Washington Coast Range: Correlation to the geomagnetic polarity time scale and implications for a long-lived Yellowstone hotspot: Geosphere, v. 10, p. 692–719, https://doi.org/10.1130/GES01018.1.

Wells, R.E., Engebretson, D.C., Snavely, P.D., Jr., and Coe, R.S., 1984, Cenozoic plate motions and the volcano-plutonic evolution of Oregon and western Washington: Tectonics, v. 3, p. 275–294, https://doi.org/10.1029/TC003i002p00275.

Wells, R.E., Jayko, A., Niem, A.R., Black, G., Wiley, T., Baldwin, E., Molenaar, K.M., Wheeler, K., Givler, R., and DuRoss, C., 2000, Geologic map and database of the Roseburg, Oregon 30 × 60′ quadrangle, Douglas and Coos counties, Oregon: U.S. Geological Survey Open-File Report OF00–376, 55 p., scale 1:100,000.

White, C.A., 1888, On the Puget Group of Washington Territory: American Journal of Science, 3rd Ser., v. 36, p. 443–450.

White, R.V., Tarney, J., Kerr, A.C., Saunders, A.D., Kempton, P.D., Pringle, M.S., and Klaver, G.T., 1999, Modification of an oceanic plateau, Aruba, Dutch Caribbean: Implications for the generation of continental crust: Lithos, v. 46, p. 43–68, https://doi.org/10.1016/S0024-4937(98)00061-9.

Widmann, P., Davies, J.H.F.L., and Schaltegger, U., 2019, Calibrating chemical abrasion: Its effects on zircon crystal structure, chemical composition and U-Pb age: Chemical Geology, v. 511, p. 1–10, https://doi.org/10.1016/j.chemgeo.2019.02.026.

Wolfe, J.A., Gower, H.D., and Vine, J.D., 1961, Age and correlation of the Puget Group, King County, Washington: Short papers in the geologic hydrologic sciences: U.S. Geological Survey Professional Paper 424-C, Article 233, p. 230–232.

Yang, G., Li, Y., Zhu, Z., Li, H., Tong, L., and Zeng, R., 2022, Seamount subduction and accretion in West Junggar, NW China: A review: Geosystems and Geoenvironment, v. 3, https://doi.org/10.1016/j.geogeo.2022.100074.